Lateral Photovoltage in Hydrogenated Amorphous Silicon And Silicon Germanium Alloys

By

ALOK SRIVASTAVA

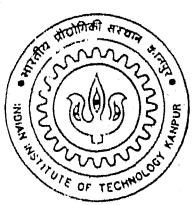

DEPARTMENT OF PHYSICS
INDIAN INSTITUTE OF TECHNOLOGY, KANPUR

December, 2000

Lateral Photovoltage in Hydrogenated Amorphous Silicon and Silicon Germanium Alloys

A Dissertation Submitted
in Partial Fulfillment of the Requirements
for the Degree of
DOCTOR OF PHILOSOPHY

By

ALOK SRIVASTAVA

to the

Department of Physics
Indian Institute of Technology Kanpur
Kanpur — 208 016, India
December 2000

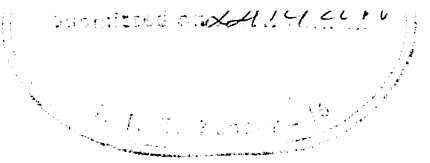

Certificate

It is certified that the work contained in this thesis entitled *"Lateral Photovoltage in Hydrogenated Amorphous Silicon and Silicon Germanium Alloys"* by *"Alok Srivastava"* is carried out under my supervision and that this work has not been submitted elsewhere for a degree.

(S. C. Agarwal)
Professor, Department of Physics
Indian Institute of Technology Kanpur
December 2000

Acknowledgements

With deep sense of gratitude I would like to say, that my association with my thesis supervisor Professor S. C. Agarwal has been a very illuminating one. I have been greatly benefitted throughout the period of my thesis work by the constant advice and encouragement that I received from him. His critical evaluation of my work has given me the chance to develop physical insight and ability to see beyond the obvious and the trivial.

I would like to acknowledge Prof. Avinash Singh, Prof. V. N. Kulkarni, Prof. V. A. Singh, Prof. Abhijit Mookarjee and Prof. Rajendra Prasad for their involvement and advice at various stages in the past.

Special thanks are due to Prof. K. K. Sharma for providing me some of the optics needed for completion of some experimental work, Dr. P. N. Dixit and Dr. R. Bhattacharya for providing me some samples used in the present study.

I wish to acknowledge my teachers at Christ Church College Dr. V. K. Srivastava, Dr. (Mrs) S. Sen, Dr. Mukul Mishra, Prof. D. S. Misra and Dr. Shailendra Kumar who tought me during M.Sc. and I must mention that it was this time when I was motivated by Prof. D. S. Mishra and Dr. Shailendra Kumar to pursue higher studies.

I am thankful to Mrs. Agarwal and Mrs. S. P. Bajpai for their affection and care.

I take this opportunity to thank Dr. S. K. Tripathi, Dr. G. S. Narayana, Dr. Pratima Agarwal, Dr. Anil Sinha, Dr. P. K. Dwivedi, Dr. S. K. Dwivedi, Mr. Manu Bajpai, Mr. Joginder Singh, and other labmates for their help and in keeping me in good humour. Thanks are also due to Dr. Ram Bilas and Mr. Rajendra for their help, whenever needed.

I am thankful to the members of Physics Workshop, Central Workshop, Glass Blowing Section, Liquid Nitrogen Plant and Physics Department office for their help.

Life of a graduate student here at IIT Kanpur is that of a near complete social isolation and I was lucky to have a few places where I could find some solace. In this regard I would like to specially thank the families of Dr. G. S. Narayana and Mr. Dinesh Deva and their playful kids and I must acknowledge Anita Bhabhi for the innumerable dinners that I had at her place.

It is also a great pleasure to acknowledge all my friends Jiten Das, Himanshu, Puranjoy, Manish, Kali Prasad, S.B. Rao, Alok Sharan, Balaji, Rajan, Amit, Tapo, Debashish, Rajesh Dwivedi, Sudhakar, Gopesh,

Brajesh Pandey, Nazrul and Sanjay Ram, who helped me in many ways and made my stay at IIT Kanpur a pleasure.

A word of special thanks for Mr. T. V. V. Ramakrishna, Dr. Pratima Agarwal and Mr. Dinesh Deva for their help in preparation of the manuscript in the present form.

In the end I would like to say that I could not have completed this work without the unending support of my younger brothers, sister and the sacrifices of my father. I hope that I shall be able to fulfill their dreams.....

Alok Srivastava

I.I.T. Kanpur

To my father

Synopsis

Hydrogenated amorphous silicon (a-Si:H) is a promising material in amorphous semiconductor industry. The material finds its applications in fabricating devices like photovoltaic cells, photoreceptors, photoconductors, thin film transistors, large area image sensors, color detectors, X-ray detectors and fluoroscopy in medical imaging and many more. This is possible because unlike other amorphous semiconductors, the density of localised states at Fermi level in a-Si:H is very low ($\sim 10^{15} cm^{-3} eV^{-1}$) and the material can be efficiently doped both p and n type by suitable addition of dopant gases prior to deposition. The absence of long range order in a-Si:H results in exponential tails of localized states in the gap whereas the dangling bonds give rise to deep gap defect states. These localized states in the gap control the electronic properties of this material and have been studied by various techniques.

The characteristics of a-Si:H based devices are found to change with prolonged use. For example, the efficiency of a-Si:H solar cells decreases and stabilizes at a smaller value after exposure to sun light for a few hours. The degradation of a-Si:H after exposure to light, commonly known as the Steabler-Wronski Effect, is found to be accompanied by an increase in the density of localized states and a decrease in the carrier diffusion length.

There have been several reports on the measurement of lateral photoeffects in a-Si:H *p-i-n* other device structure. In these studies, the devices are reverse biased and one finds a photovoltage between two coplanar electrodes, as the space between them is illuminated by a laser spot. This lateral photovoltage (LPV) depends on the position of the spot. We found that a large LPV appears between two coplanar electrodes on intrinsic a-Si:H thin films with no *p-i-n* structure. Also, the open circuit voltages are as high as hundred millivolts. This is quite interesting since this indicates the possibility of using a-Si:H as a large area position sensitive detector.

We have measured LPV as a function of temperature for different positions of illumination on a-Si:H and a-SiGe:H samples. The position dependence of LPV is qualitatively similar in all cases while the magnitudes differed from sample to sample. Also, LPV decreases as the measurement temperature increases. One may try to understand the observed LPV as follows: when the sample is illuminated nonuniformly, a diffusion of the photogenerated carriers occurs towards the

low concentration (dark) region. Since the diffusion lengths of electrons and holes are different, they setup different charge profiles, and if the illuminated region is situated closer to one of the electrodes than the other, this gives rise to the observed LPV. In order to understand the relationship between diffusion lengths of carriers and LPV, we measured the ambipolar (hole in a-Si:H) diffusion length by the Steady State Photocarrier Grating (SSPG) technique. We found that when the samples are light soaked (LS) by exposure to a uniform strong illumination for a long time, the diffusion length decreases. This is in agreement with the published results. However, contrary to our expectations, LPV increases. Further, the magnitude of LPV is much larger than estimated from a suitable model. This is makes LPV an interesting problem to study.

An analysis of LPV is done in terms of diffusion of photogenerated electrons and holes. The charge profiles of electrons and holes are determined from the diffusion lengths and number of photogenerated carriers during LPV measurements. It turns out that whereas the position dependence of LPV can be explained qualitatively the calculated magnitude of LPV is much smaller than observed. We propose that the observed large magnitude of LPV has to do with the heterogeneities present in the samples. This model can also account for the behaviour of LPV upon light soaking.

Organization of the Thesis

The thesis is divided in six chapters. The first chapter describes in brief the electronic properties of hydrogenated amorphous silicon, and discusses the rigid band and potential fluctuation models which have been proposed to explain its properties. Various interesting photoeffects observed in semiconductors are discussed. An introduction to our studies of Lateral Photovoltages in a-Si:H and a-SiGe:H thin films is also presented here. The second chapter describes the preparation of a-Si:H and a-SiGe:H samples by glow discharge technique. The structural, electrical and optical characterizations are presented alongwith a brief description of the setup used for band gap, density of states, dark and photoconductivity measurements. The experimental setup used for LPV as well as Steady State Photocarrier Grating (SSPG) techniques are also described. The principle and theory of the Steady State Photocarrier Grating technique are presented in Chapter 3 and an expression for the estimation of ambipolar diffusion length of photocarriers is given. The results of the SSPG and LPV experiments carried out on a-Si:H and a-SiGe:H samples in annealed as well as light soaked states are presented in Chapter 4. An analysis for the LPV is presented in Chapter 5 and the problems like large magnitude and increase after light soaking in LPV are discussed. A model to explain the observed results of LPV in terms of the heterogeneities and potential fluctuations present in the material is also presented in this

Chapter. The last Chapter presents the summary and conclusions of the present study. Directions for future work, which may help in further understanding the LPV are also suggested in this chapter. The references to the literature cited are listed at the end of the thesis.

CONTENTS

List of Figures

List of Tables

CHAPTER

ONE

Introduction

Amorphous silicon films prepared by glow discharge decomposition of silane [1, 2] differ in many respects from evaporated amorphous semiconductors. The evaporated amorphous semiconductors show very small photoconductivity and are insensitive to doping. In contrast, amorphous silicon prepared by glow discharge shows activated dc conductivity, a good photoconductivity and efficient doping by addition of phosphine or diborane to the silane gas prior to decomposition [2]. The high defect density of amorphous silicon prepared by evaporation is responsible for this difference. Presence of hydrogen in amorphous silicon prepared by glow discharge was confirmed by Triska et al [3] and Fritzsche

in bond angles and bond lengths results in the tailing of band edges in the forbidden gap. In addition to this, some electronic states in the gap arise from the coordination defects like dangling bonds. These defects determine many electronic properties by controlling trapping and recombination.

The presence of disorder and defects (dangling bonds) gives rise to localized electronic states in the band gap. Because of these localized states, the energy gap looses its meaning in amorphous semiconductors. The disorder also affects mobility of charge carriers which is drastically reduced in the localized states. Thus, instead of energy gap, we talk of mobility gap in amorphous semiconductors. The Mott-CFO model [16]for the distribution of the density of states in the mobility gap is shown schematically in Fig. 1.1 [17]. This density of states picture is also termed as the the rigid band picture. This is due to the fact that the energy of the conduction or valence band mobility edges remains fixed with respect to the Fermi level which is in the middle of the mobility gap.

Although, various electronic properties of hydrogenated amorphous silicon could be successfully explained by this model, there are some observations that could be better understood in term of the potential fluctuation model [18], which is described below. For example, it is easier to understand the difference between the activation energy of dark conductivity and the slope of thermoelectric power of a-Si:H in terms of potential fluctuations. Also, it becomes obvious that the electrical and

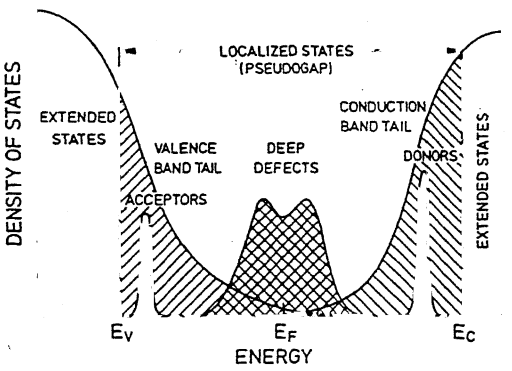

Figure 1.1: Schematic density of states distribution in the gap of a real amorphous semiconductor. After ref. 17.

optical gaps need not be the same as they measure differents aspects of the electronic structure.

1.2 The Potential Fluctuation Model

The a-Si:H grown by the glow discharge of silane has an inhomogeneous structure. The structural inhomogeneities [19, 20] may be caused by local density fluctuations, growth inhomogeneities [21] and charged centers [18]. Proton resonance experiments by Reimer et al [22] show that hydrogen, which is about 8-10 atomic %, is distributed inhomogeneously in a-Si:H. Nearly 4 atomic % hydrogen is present in a dilute monohydride phase and the rest is in a clustered hydride phase with

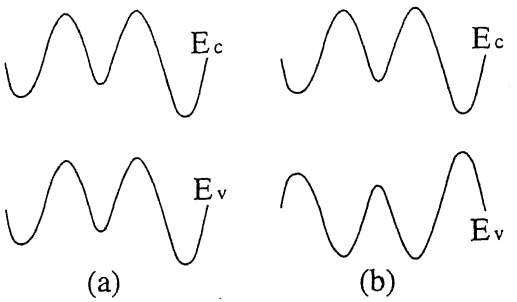

Figure 1.2: Potential energies in Conduction and Valance bands with long-range fluctuations (a) inelastic, arising from electrostatic charges which may be charged defects or dopants or both depending on whether the material is doped or not and (b) elastic fluctuations arising from variation in composition from place to place in the material. After ref. 15.

5-7 atoms per cluster, which resembles a di- or trivacancy whose internal surface is dressed with hydrogen. These heterogeneities give rise to long range potential fluctuations which can be visualized as spatial variations in the energy of valence and conduction band mobility edges with respect to the Fermi level (see Fig. 1.2).

The charged defects can produce potential fluctuations of an electrostatic nature if there is an spatial variation in the charge density. In this case the variation in potential energies of conduction and valance band are not accompanied by the variation in the band gap as in the case of elastic fluctuations Fig. 1.2(a). The films of Si and Ge are

known to contain voids and if any of these remain charged after reconstruction of unsatisfied orbitals such potential fluctuations will result [15, 18, 23]. In doped a-Si:H, an inhomogeneous distribution of dopants may give rise to additional potential fluctuations [24] of this kind.

The local variation in composition produces the so called elastic fluctuations in the band gap [15] in which the gap varies from place to place as shown in Fig. 1.2(b). For example, the variation in hydrogen content in a-Si:H results in spatial variation of the band gap from 2eV in clustered phase to 1.3eV in the dilute phase [25].

Taking into account these potential fluctuations, Fritzsche proposed a model which is commonly known as the "Potential Fluctuations Model". According to this model, the regions in which predominantly holes are localized are not the same regions in which electrons are localized. This model further suggests that, one should distinguish between three kind of states: (i) states localized in certain regions, (ii) channel states which extend through the material but are excluded from certain regions, and (iii) extended states which describe electrons for which the probability to be found anywhere in the material is finite [18].

The potential fluctuation model has been invoked to explain a variety of results in hydrogenated amorphous silicon and other materials which could not be explained by the rigid band model [18, 24, 26–34].

Hydrogenated amorphous silicon has been studied extensively by various techniques, e.g., luminescence [35], electron spin resonance

[36], field effect measurements [37], thermally stimulated currents [38–43], capacitance techniques [44], and sub-gap absorption using constant photocurrent method (CPM) and photothermal deflection spectroscopy (PDS) [45–50] etc. These studies have led to our present day understanding of the density of localized states in this material. In addition to these, measurements like conductivity, photoconductivity and thermoelectric power have been done to understand the transport properties of a-Si:H. The conductivity and thermopower measurements have also been used to estimate potential fluctuations [24, 32, 33]. These measurements have helped in understanding the thermal and light induced (Steabler-Wronski effect) metastabilities [33] that the width of potential fluctuations increases after LS. The present thesis is on the measurements of Lateral photovoltage in a-Si:H and a-SiGe:H alloy thin films. It turns out that our LPV results can be better understood in terms of the potential fluctuations model.

1.3 Lateral Photovoltage in a-Si:H

One of the well studied photovoltaic effects in a-Si:H and a-SiGe:H films is the surface photovoltage (SPV) which is defined as the change in the surface potential due to illumination. This effect, observed at Si and Ge surfaces, was first reported by Brattain [51] and was followed in detail by Brattain and Bardeen [52]. The SPV induced at the free

surface of a semiconductor sample with a grounded Ohmic back contact has been a subject of extensive research in a-Si:H and alloys [53–62].

The photovoltaic effects like SPV are measured when the films are under uniform illumination. However, not much work exists on photovoltage measurements with films under nonuniform illumination. When the effect of nonuniform illumination is measured in a direction perpendicular to that of illumination, we have the so called the lateral photoeffect.

Lateral photoeffects had been the subject of the investigation on different materials and device structures by Lucovsky [63], Noorlag and Middelhoek [64], Connors [65] and Woltering [66]. Several reports have appeared in the literature on the measurement of LPV on a-Si:H *p-i-n* devices under reverse bias which are reported to function as position sensitive detectors [67–71].

We have found large Lateral Photovoltage (LPV) in intrinsic layers of a-Si:H and a-SiGe:H by illuminating them with a laser spot [72–74]. This is interesting since in our case no *p-i-n* like structure is required and the magnitude of LPV is as high as 100 mV in some cases. In this setup, a potential difference is generated between two coplanar electrodes on a-Si:H and a-SiGe:H films when a small region between these electrodes is illuminated. One may try to understand the observed LPV as follows: when the sample is illuminated nonuniformly, diffusion of the photogenerated carriers occurs towards the low concentration (dark) region. As the diffusion lengths of electrons and holes

are different, they setup different charge profiles, and if the illuminated region is situated closer to one of the electrodes than the other, this gives rise to the observed LPV. Though, this appears to be similar to Dember voltage [75], the magnitudes are far higher than those can be attributed to Dember voltage. In all cases the LPV decreases with increasing measurement temperature. We also found that when the sample is light soaked (LS) by exposing it to uniform strong illumination for a long time, the diffusion length decreases as in the published works [10, 76–78], whereas, contrary to our expectation, LPV increases. These observations make LPV an interesting phenomenon to study the physics involved. An attempt is made to explain the large magnitude of LPV in terms of the heterogeneities and potential fluctuations in a-Si:H. Some of the interesting photovoltaic effects, observed earlier in different materials, are briefly described below.

1.4 Other Photovoltaic Effects

In the context of the present work it is worthwhile to mention different photovoltaic effects, like Dember effect, lateral photoeffects and photoangular effect in different device structures. While it is possible to offer a simple explanation for the Dember effect and lateral photoeffect as described below, high-voltage photovoltaic effects [79] and photoangular effect [80] observed in some semiconductors are highly anomalous and cannot be easily explained. Anomalous photovoltaic

effects have been observed in a large number of semiconductor (for a review see [75]) films and even in single crystals of ZnS [81,82] and sulphur [83]. Photovoltages as high as hundreds of volts were obtained [84] and it was shown that the voltage is generated continuously along the length of the film and is not a contact effect [79].

1.4.1 Dember Effect

Strongly absorbed radiation generates a high density of electron-hole pairs at the surface of a semiconductor. The photogenerated carriers diffuse away from the illuminated region. The carriers having higher mobility, will extend somewhat farther into the bulk than those with the lower mobility. When electrons are more mobile than holes, in the absence of any other effect, the differential diffusion will tend to make the surface more positive than the bulk. The direction of the resulting electric field is such as to accelerate the lower-mobility carriers (holes) and slow down the more mobile carriers, so that the net current is zero. In this condition, the potential difference between the front (illuminated) and the back surface is the Dember voltage [75] and it is usually of the order of millivolts. Dember discovered this effect along the semiconductor between illuminated and dark regions [85,86].

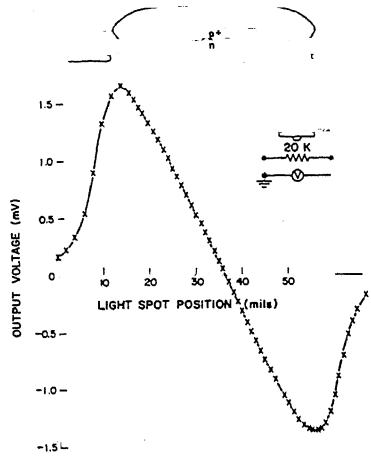

Figure 1.3: Lateral Photovoltage curve for p^+ on n photocell as observed by Wallmark. After ref. 75.

1.4.2 Lateral Photoeffect on p-n Junctions

Lateral Photoeffect was reported by Schottky in 1930 [87] and by Wallmark [88, 89]. Wallmark studied lateral photoeffect in a direction parallel to the p-n junction. The device consisted of two ohmic contacts on either side of a floating p-n junction, as shown at the top of Fig. 1.3. Because the p^+ region has high conductance, it forms an equipotential surface. The normal "photovoltage" due to small light spot forward biases the p-n junction. The excess holes can leak out of the p^+ region over the whole junction area. If the light spot illuminates the center of the junction, the hole current flows symmetrically out of the junction

and no net voltage appears across the ohmic contacts. If, on the other hand, the light spot illuminates the left side of the junction, most of the holes leak out of the right side of the junction, making the right more positive than the left side. Electrons in the n-type region redistribute themselves to preserve local charge neutrality. This charge redistribution generates a voltage across the two ohmic contacts. The polarity of the lateral photovoltage reverses when the light spot illuminates the right side of the junction.

1.4.3 Anomalous Photovoltaic Effects

Some semiconductors in the form of thin films exhibit a high-voltage photovoltaic effects. Goldstein and Pensak observed photovoltages as high as 400Volts in CdTe films of about $1\mu m$ thickness [79]. Although this phenomenon is spectacular and very intriguing, very little progress has been made in explaining it in a definitive way. The anomalous photovoltaic effect has been observed in a large number of semiconductors films [75] and even in single crystals of ZnS [81, 82] and Sulphur [83].

The main requirement for the occurance of this effect is that when the film is grown, the insulating substrate must be inclined with respect to the gradient of the incident vapor. It has been shown experimentally that it is not a contact effect and the end of the film nearest

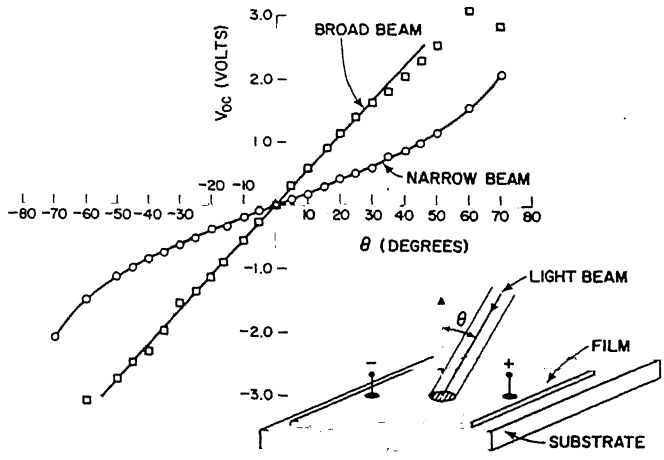

Figure 1.4: Variation of open-circuit photovoltage with the angle of incidence as observed on polycrystalline GaAs and Si films. After ref. 75.

the evaporator is almost always negative [79]. Moreover, the variation in the film thickness due to angular deposition is not a relevant factor [90].

In addition, anomalous photovoltaic effects have been observed in the films prepared at normal incidence of incident vapour. Photoangular effect is an example of such anomalous photovoltaic effect observed in GaAs and Si thin films. These effects have been observed on thick films (2-50μm) [80]. When the film is illuminated at normal incidence, no photovoltage appears. As the light beam is tilted with respect to a normal to the film, in the the plane passing through the two small electrodes (Fig. 1.4), a photovoltage appears and grows with further inclination of the beam. The photovoltage has opposite polarities on either side of normal incidence. Sometimes the potential difference developed is larger than the energy gap of the semiconductor [75]. The tentative models proposed to explain these effects are based on the summation of elementary photovoltages generated at grain boundaries in the films.

1.5 Organization of the Thesis

The next chapter describes the preparation of a-Si:H and a-SiGe:H samples by glow discharge technique. The structural, electrical and optical characterizations are presented alongwith a brief description of the setup used for band gap, density of states, dark and photoconductivity measurements. The experimental setup used for LPV as

well as Steady State Photocarrier Grating (SSPG) techniques are also described. The principle and theory of the Steady State Photocarrier Grating technique is presented in the Chapter 3 and an expression for the estimation of ambipolar diffusion length of photocarriers is given. The results of the SSPG and LPV experiments carried out on a-Si:H and a-SiGe:H samples in annealed as well as light soaked states are presented in the Chapter 4.

An analysis for the LPV is presented in the Chapter 5 and the problems like large magnitude and increase after light soaking in LPV are discussed. A model to explain the observed results of LPV in terms of the heterogeneities and potential fluctuations present in the material is also presented in this Chapter. The last Chapter presents the summary and conclusions of the present study. Directions for future work, which may help in further understanding the LPV are also suggested in this chapter. The references to the literature cited are listed at the end of the thesis.

CHAPTER

TWO

Experimental

An account of preparation and preliminary characterization of the samples used in the thesis is given in this chapter. In addition to this, the main experiments viz Steady State Photocarrier Grating (SSPG) and Lateral Photovoltage (LPV) carried out for this work are also described.

2.1 Sample Preparation

Samples in the form of thin films are deposited by the standard radio frequency Glow Discharge technique [91–93] where a mixture of silane (SiH_4) and hydrogen (H_2) gases is decomposed by the application of r.f. power. A mixture of SiH_4, GeH_4 and H_2 is used to make a-SiGe:H films.

Corning 7059 glass is used as the substrate as it has higher resistivity compared to that of hydrogenated amorphous silicon. Also, it is transparent in the energy range from 0.6eV to 4.0eV making it suitable for the optical studies of a-Si:H films. The details of film deposition are described here.

2.1.1 Substrate Cleaning

Substrate cleaning is an important step, as the adherence of a-Si:H to the substrate and the sample uniformity are largely dependent on the condition of the substrate. Preliminary cleaning is carried out by washing with detergent followed by ultrasonic cleaning in acetone and methanol. The substrate is finally vapor degreased with isopropyl alcohol and immediately transferred to the deposition chamber of the r.f. glow discharge system (Fig. 2.1).

2.1.2 Deposition of a-Si:H and a-SiGe:H Films

The setup for the deposition of hydrogenated amorphous silicon films is shown in Fig. 2.1. The deposition chamber is initially evacuated below 10^{-7} torr using a turbo molecular pump and simultaneously baked at about 300°C for two hours to remove the adsorbed impurities. The system is then purged with high purity hydrogen gas followed by the hydrogen plasma cleaning of the substrate.

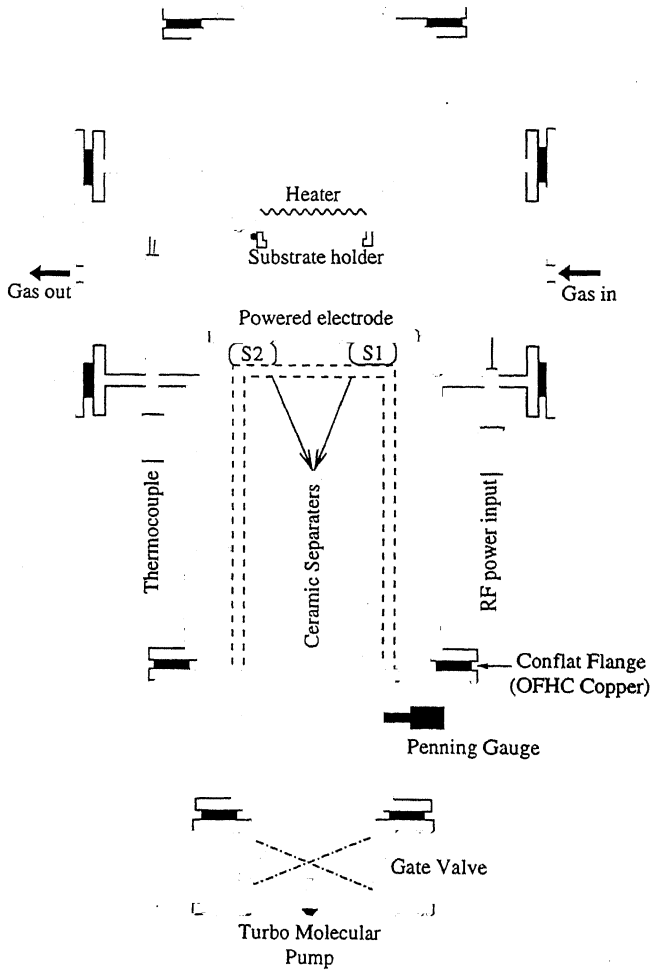

Figure 2.1: Schematic of R.F. Glow Discharge Deposition System used for making the a-Si:H films.

A mixture of silane (SiH_4) and hydrogen is introduced in the chamber at a constant flow rate of about 20sccm and r.f. (13.56 MHz) power is applied. Silane molecules are dissociated into neutral radicals, atoms and ions due to collision with energetic electrons in the plasma. These molecules, atoms and ions travel to the surface of the substrate through a gas phase diffusion process resulting in the deposition of hydrogenated amorphous silicon thin film [94].

The a-Si:H sample (s1) is deposited at about 275°C using a 10:90 mixture of silane and hydrogen flowing at 20sccm. The substrate temperature is kept between 250°C and 300°C during deposition to obtain device quality films [95]. The r.f. power density and chamber pressure are about $40mW/cm^2$ and 1 torr respectively. The samples s2, s3 and s4 are deposited under identical conditions with varying germanium content. Germanium content in the film is varied by changing the GeH_4 flow while the total flow rate is kept fixed at 40sccm. These samples are deposited at 350°C with total reactant gas pressure 0.6 torr and r.f. power about $10mW/cm^2$.

With these parameters, the deposition rate of the films is about 1 $Å/s$ and the preliminary characterization of the films reveals that these are of device quality.

2.1.3 Electrical Contacts

Coplanar electrodes consisting of 1cm long rectangular strips of NiCr deposited by thermal evaporation under vacuum on the top of the film. The separation of these electrodes is about 1mm for the conductivity, CPM and SSPG measurements whereas it is about 20mm for the Lateral Photovoltage measurements. Sometimes, silver paint electrodes, in a geometry similar to that of the nichrome electrodes, are also used.

Both type of contacts show an Ohmic behaviour in the current-voltage (IV) measurement for applied field upto 1000V/cm in the temperature range of our measurements ($300K < T < 450K$).

2.2 Sample characterization

The samples are characterized to check the quality of the films and the parameters like activation energy (E_σ), optical gap (E_g), density of states etc match favorably with those of the device quality films.

2.2.1 Structural Characterization

The amorphous nature of the films is verified by the x-ray and electron diffraction studies. The X-ray diffractograms show a broad peak whereas the electron diffraction has two diffused rings. This indicates that the films are amorphous in nature.

2.2.2 Electrical Characterization

The dark conductivity (σ) and photoconductivity (σ_{ph}) are measured. The activation energy (E_σ) is obtained from the temperature dependence of conductivity.

Conductivity and Activation Energy Measurement

The electrical characterization is carried out in a high vacuum system consisting of a stainless steel chamber (Fig. 2.2) equipped with a sample holder with heating arrangement. The sample can be illuminated through a quartz window for the photoconductivity and LPV measurements. The temperature is measured with a thermocouple mounted on a dummy sample kept near the sample.

The conductivity is measured in the above setup under a vacuum of $\approx$ 10^{-6}torr. The samples are slowly heated from room temperature 300K to 450K and sample current (I) is recorded as function of temperature for a constant applied voltage of 100V. The process is repeated while slow cooling the sample. Activation energy is obtained from the slope of log(I) vs 1/T plot of the data. The intensity dependence of photoconductivity for the samples is measured using a 360W tungsten halogen and neutral density filters. A heat reflector and a water filled beaker are used to prevent the heating of the sample during

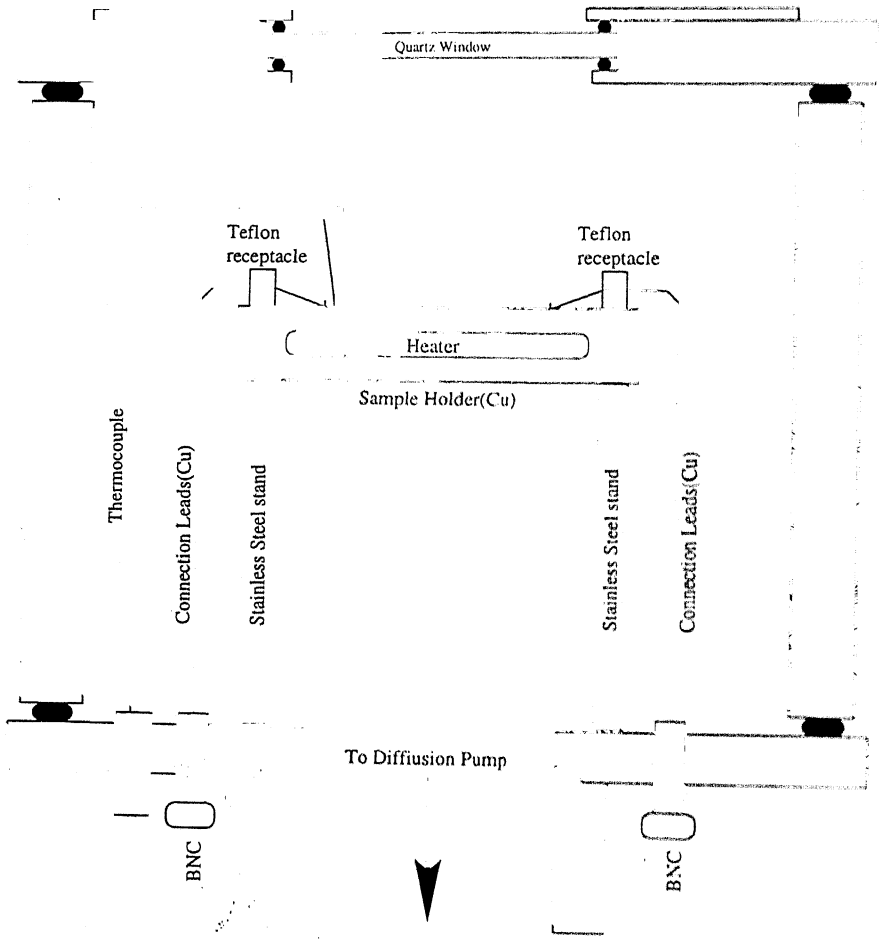

Figure 2.2: Schematic of the setup used for the electrical characterization and Lateral Photovoltage measurements.

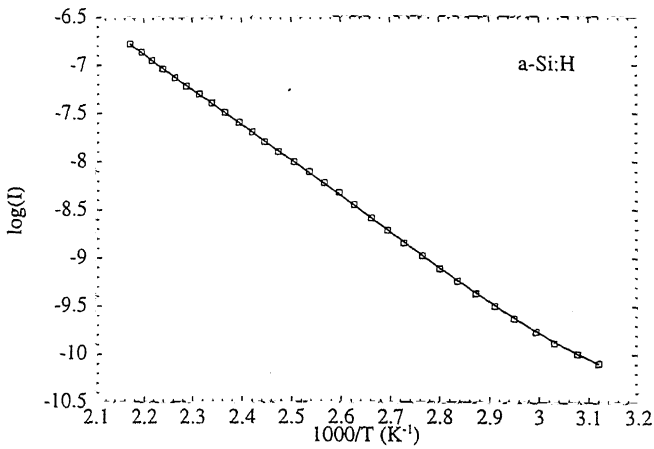

Figure 2.3: Typical plot of log(I) as a function of inverse of temperature for one of the samples studied.

the measurement. The intensity is varied over several orders of magnitude and photocurrent is measured for a constant applied voltage of 100Volts.

The parameters σ_d, σ_{ph}, E_σ and the exponent γ of the intensity dependence of photoconductivity ($\sigma_{ph} \propto F^\gamma$ where F is the intensity of illumination) are given in the Tables 2.1 and 2.2.

2.2.3 Optical Characterization

Subgap absorption (α) is measured by Constant Photocurrent Method (CPM) for the determination of the density of states measurement. The parameters like thickness of the film and absorption coefficient α

are determined from the optical transmission in the wavelength range 330nm-1450nm (3.78eV-0.86eV).

2.2.3.1 Transmission Measurement

The setup for transmission measurements, shown in the Fig. 2.4, consists of a grating monochromator (Bausch & Lomb) equipped with a 75Watt quartz halogen lamp, a lock-in amplifier (SR-510) a calibrated Si photodiode and an optical chopper. A Monochromatic beam, chopped at 13Hz, is made to fall on the sample and the transmitted intensity is measured using the photodiode and the signal is measured by the lock-in amplifier for different values of the wavelength (λ). A high pass order sorting filter (Hoya-64) is used to remove the second order grating diffraction from the monochromator output. The transmission data is analyzed to get the absorption coefficient $\alpha(\lambda)$, optical gap E_g and the thickness (d) of the films [96].

2.2.3.2 Film thickness calculation

The thickness of films is determined from the transmission data using the formulation of Swanpole [96]. The transmission T(λ) is a function of the wavelength λ, refractive indices n and s of the film and substrate (Corning 7059) respectively, the absorption coefficient α and the film thickness d: $T = T(\lambda, s, n, d, \alpha)$. The interference condition for the maximum and minimum is $2nd = m\lambda$ where m is an integer for maxima and a half integer for minima. If n_1 and n_2 are the refractive

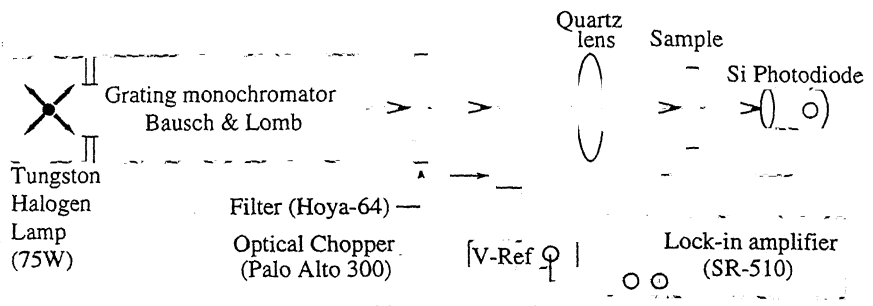

Figure 2.4: Schematic of the setup used for the transmission measurements on a-Si:H and a-SiGe:H sample.

indices at the two adjacent maxima or minima at λ_1 and λ_2 respectively, then

$$d = \frac{\lambda_1 \lambda_2}{2(n_2\lambda_1 - n_1\lambda_2)}. \tag{2.1}$$

For an adjacent maximum at λ_1 and minimum at λ_2, the interference conditions are

$$2n_1 d = m\lambda_1 \tag{2.2}$$

and

$$2n_2 d = (m + 1/2)\lambda_2 \tag{2.3}$$

which give

$$d = \frac{\lambda_1 \lambda_2}{4(n_2\lambda_1 - n_1\lambda_2)}. \tag{2.4}$$

From the above equations the thickness d is calculated for various pairs of maxima or minima. The average value d_{av} is calculated and substituted in the Eq. (2.2) and Eq. (2.3) and the resulting equations

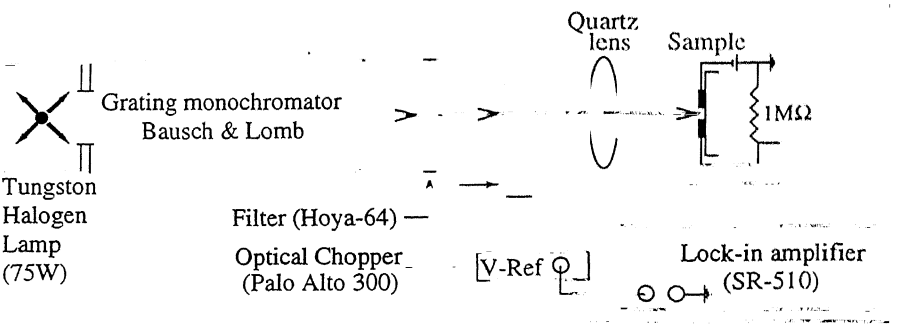

Figure 2.5: Schematic of the setup for the Constant photocurrent method used for the determination of density of states.

are solved for m. This value of m is approximated to the nearest integer and used to recalculate the refractive indices n. The values of n_1 and n_2 so obtained are substituted back into the Eq. (2.1) to recalculate d_{av}. The value of d so obtained is the correct film thickness. The details of the calculation of refractive indices $n(\lambda)$ and the absorption coefficient α are given in the Appendix A.

2.2.3.3 Density of States Measurement

The Constant Photocurrent Method (CPM) is used to determine the density of states in our samples. This method actually measures the absorption coefficient α as a function of wavelength. The absorption coefficient $\alpha(h\nu)$ for transition from initial state g_i to the final state

g_f, separated by energy $h\nu$, is given by [97]

$$\alpha(h\nu) = \frac{C}{h\nu} \int g_i(\epsilon) f(\epsilon) g_f(\epsilon + h\nu)[1 - f(\epsilon + h\nu) d\epsilon].$$

The density of states is estimated from the spectral dependence of α by the method described by Kočka et al [97].

The schematic setup for the CPM is shown in Fig. 2.5. The CPM setup consists of a grating monochromator, optical chopper and a Lock-in amplifier. Light from the monochromator is passed through a filter to cutoff the second order diffraction and chopped at 13Hz before it falls on the sample and the photocurrent is measured as a voltage drop across a 1MΩ resistance. A suitable value of photocurrent is chosen and is kept constant for all the wavelengths by changing the intensity of light.

For undoped a-Si:H, the photocurrent is mainly contributed by electron current because the $\mu\tau$ product is about 10 times smaller for holes than electrons [97]. The photocurrent density J_n is given by [98]

$$J_n = e\, n_{ph}\, \eta\, \mu\, \tau\, (1 - R)\, \{1 - exp(-\alpha d)\} \left(\frac{F}{L}\right) \qquad (2.5)$$

where e is the electronic charge, n_{ph} the number of incident photons per unit area per unit time, R the reflection coefficient, d the film thickness, η the photogeneration efficiency, μ the electron mobility, τ the mean life time of electrons (recombination lifetime), F the applied electric filed and L is the separation between the electrodes.

In the subgap region R varies slowly with energy and is assumed

to be constant; the $\mu\tau$ product, which generally depends upon the position of quasi Fermi level, is also constant as the photocurrent is kept constant in CPM, the value of η is $\approx$ 1 at $300K$ [97]. Moreover, for the subgap region $\alpha d \ll 1$ which reduces $[1 - exp(-\alpha d)]$ to $\alpha\, d$ and under these approximations we have

$$J_n = constant \times \alpha\, n_{ph}$$

which gives

$$\alpha(h\nu) = \frac{constant}{n_{ph}(h\nu)}.$$

Thus a plot of inverse of the intensity required to keep photocurrent constant with $h\,\nu$ is same as the plot of α with $h\,\nu$ within a factor of a constant which can be obtained by matching the CPM curve with the α obtained from the transmission at higher energies where $\alpha\, d \approx 1$.

Fig. 2.6 shows a typical plot of $\alpha(h\nu)$ vs $h\nu$ as estimated from CPM for our samples and the density of states for the samples are given in the Table 2.1. These are comparable to those of the device quality a-Si:H samples reported in the literature for which it is about $2 \times 10^{15}\text{cm}^{-3}$ [97].

2.3 The SSPG Setup

2.3.1 Principle

The SSPG technique involves measurement of photocurrents by illuminating the sample with two coherent beams of unequal intensity from

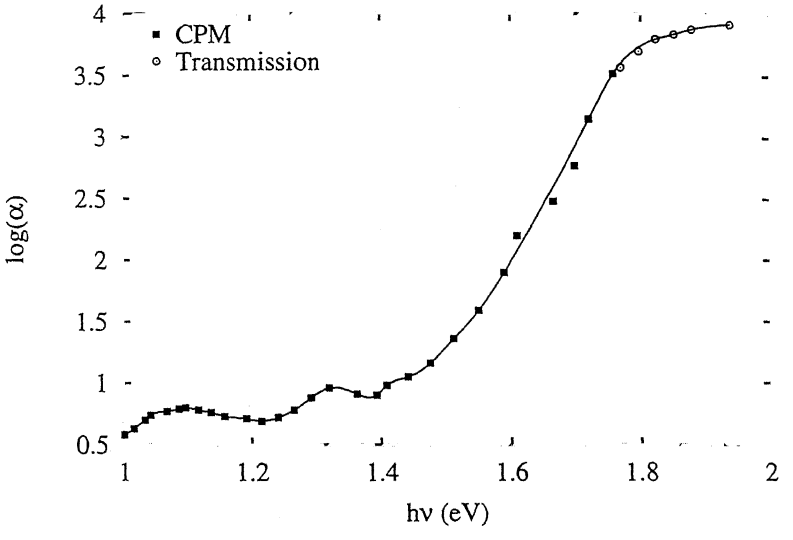

Figure 2.6: Typical plot of absorption coefficient $\alpha(h\nu)$ as a function of energy obtained from the constant photocurrent method.

Table 2.1: Parameters like optical gap (E_g), density of states (DOS) and the exponent of the intensity dependence of photoconductivity (γ) of the a-Si:H and a-SiGe:H samples. Here Ge% = [GeH_4/ (SiH_4 + GeH_4)] $\times$100.

Sample	Ge%	E_g (eV)	DOS ($cm^{-3}eV^{-1}$)	γ
s1 (a-Si:H)	0	1.70	1×10^{16}	0.75
s2 (a-Si:H)	0	1.73	1×10^{15}	0.98
s3 (a-SiGe:H)	10	1.51	1×10^{16}	0.83
s4 (a-SiGe:H)	20	1.48	3×10^{16}	0.90

Table 2.2: Parameters like activation energy (E_σ), dark conductivity (σ_d), photoconductivity (σ_{ph}), of the a-Si:H and a-SiGe:H samples. Here Ge% = [GeH_4/ (SiH_4 + GeH_4)] $\times$100.

Sample	Ge%	E_σ (eV)	σ_d ($\Omega^{-1}cm^{-1}$)	σ_{ph} ($\Omega^{-1}cm^{-1}$)
s1 (a-Si:H)	0	0.75	1.2×10^{-10}	8.2×10^{-5}
s2 (a-Si:H)	0	0.92	1.0×10^{-10}	1.4×10^{-4}
s3 (a-SiGe:H)	10	0.85	8.9×10^{-12}	1.9×10^{-8}
s4 (a-SiGe:H)	20	0.82	6.7×10^{-12}	5.0×10^{-9}

a polarized laser. The beams can be made to produce uniform illumination or an optical grating on the sample by making their polarization perpendicular or parallel with each other. The stronger of the two beams provides a uniform background illumination in the interference condition whereas the weaker beam interferes with an equal part from the stronger beam. The weaker beam is chopped and photocurrent due

to this beam is measured in both the conditions when the beams interfere or produce a uniform illumination. The ratio of the photocurrent in the interference condition to that in noninterference, designated by β, and the optical grating period Λ are related by the following [76]

$$\beta = 1 - \frac{2\phi}{[1 + (2\pi L/\Lambda]^2} \tag{2.6}$$

where ϕ is a constant and L is the ambipolar diffusion length of the photocarriers [76].

For determination of L, β is measured at various grating periods Λ, which depends upon the angle between the two beams I_1 and I_2. The total intensity of light falling on the sample is constant in this experiment.

2.3.2 Experimental Details

The schematic of the SSPG setup used is shown in the Fig. 2.7. A laser beam from a 5mW linearly polarized He-Ne laser (wave length 632.8 nm) is split in two with intensities I_1 and I_2 using a beam splitter (BS) and the intensity of the beam I_2 is reduced by a factor of 10 with respect to I_1 with the help of a neutral density filter (ND).

It was observed that the beam splitter BS introduced a change in the planes of polarization of the two laser beams I_1 and I_2 and the two are not copolarized. In addition to this, the mirrors M1 and M2 also introduced a change in the plane of polarization of the two beams in an uncorrelated manner. Moreover, this change was found to depend

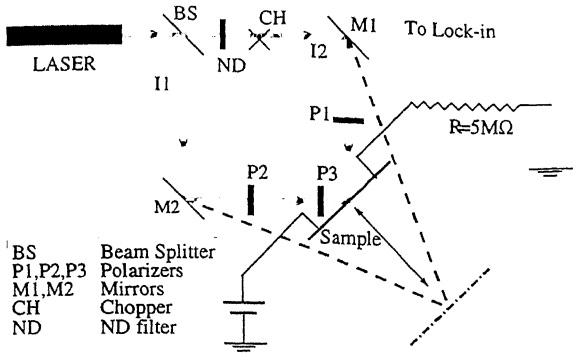

Figure 2.7: The schematic setup of the Steady State Photocarrier Grating Measurement.

on the angle of incidence of the beams on the mirrors. Thus a simple setup consisting of a polarized laser and a half wave plate as shown in [76, 77] would have given erroneous results.

In order to be to sure that the beams are copolarized and crosspolarized for all the grating periods, without any change in the total intensity, a set of polarizers are placed in the path of beams just before the beams fall on the sample as shown in the Fig. 2.7. The interference and uniform illumination (noninterference) conditions are obtained as described here.

The axis of polarization of the polarizer P2 is made parallel to the plane of polarization of the beam I_1 after the beam is reflected from the mirror M2. The polarizer P3 is now placed in the path of the beam I_1 and is rotated so that it passes no light. In this situation, the two

polarizers have their axis of polarization perpendicular to each other. This angular setting of the polarizer P3 is marked as zero on its circular scale. If P3 is now rotated by 45° on either side of its zero position, i.e, to 45° or 315°, it passes same intensity but the planes of polarization in the two settings are normal to each other. P3 is now set to 45° and placed in the path of the beam I2 and P1 is now placed in the path of the beam I2 emerging from P3. P1 is now rotated till the transmitted light goes to zero and this position of polarization of P1 is fixed through out the experiment and P3 is brought back to its original position in the path of the beam emerging out of P2. A suitable ND filter is now placed in the path of beam I2 (before P1) so as reduce the intensity of this beam.

Thus, the position of P3 at 45° and 315° correspond to noninterference and interference conditions respectively. The beam I_2 is chopped and the a.c. photocurrents in the interference ($I^{\parallel}_{ph}$) and noninterference ($I^{\perp}_{ph}$) conditions are measured as a voltage drop across a series resistance R ($\sim$ 5MΩ) using a lock-in amplifier (SR510) as shown in the Fig. 2.7.

2.4 Lateral Photovoltage Measurements

When a laser beam is shone on an a-Si:H film between the two electrical contacts 1 & 2 as shown in the Fig. 2.8, an open circuit voltage is detected between these contacts. As this photogenerated potential

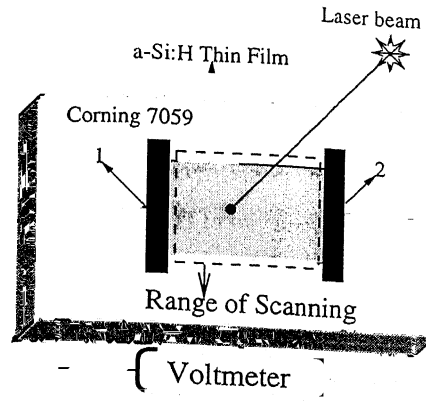

Figure 2.8: Sample and the electrode geometry for the measurements of Lateral Photovoltage. The dark bands are Teflon coated metal strips covering nichrome electrodes 1 & 2 to avoid contact photovoltage.

difference appears along the length of the sample, we term it as the Lateral Photovoltage ($\boldsymbol{LPV}$).

For this measurements, evaporated nichrome and silver paint have been used, in a coplanar geometry, as electrical contacts. These electrodes are about $6mm$ long and 20mm apart. The measurements are carried out in a vacuum chamber equipped with a quartz window and heating arrangement (Fig. 2.2). A low power ($3mW$) semiconductor diode laser (673nm), mounted on a traveling microscope, acts as the source of illumination. The traveling microscope is used to move the laser beam along the length of the sample. This $\boldsymbol{LPV}$ is measured

with a Keithley-617 electrometer for different positions of the light spot along the sample.

The measurements are performed above room temperature in the range of 390K-450K. The LPV measurements below 390K are not reported as these are too noisy because of the high impedance of the sample.

Uniformity of temperature along the sample is very crucial in this experiment as the lack of it produces a very large thermoelectric emf which must be avoided. Temperature uniformity is achieved by keeping the sample in good thermal contact with the sample holder and by waiting at the measurement temperature till the thermoelectric signal, if any, is reduced to zero. The thermalization is done in dark and LPV is measured only when there is no thermoelectric signal.

The electrical contacts are kept in dark using Teflon coated metal strips as shown in Fig. 2.8. This is to avoid any contact photovoltage from the diffused light during the illumination by the laser.

CHAPTER

THREE

Steady State Photocarrier Grating Technique

The analysis of lateral photovoltage as presented in the Chapter 5.1 requires the knowledge of diffusion lengths of photocarriers. Several techniques e.g. Surface Photovoltage [53–56, 99–104], Transient Grating [105–108] and Steady State Photocarrier Grating (SSPG) [76, 109] have been developed for their measurements. We have used the SSPG technique to estimate the ambipolar diffusion length, which equals the hole diffusion length, in the samples studied for this thesis. The theory of this technique (SSPG) is briefly outlined here.

SSPG technique involves measuring the conductivity of the sample with two beams of intensity I_1 and I_2 falling on it. It is already mentioned that $I_1 \gg I_2$ (See Sec 2.3.1) and the polarization of beams is

adjusted so that beams can interfere or produce uniform illumination. The beam I_2 is chopped and if $\sigma(I_1 + I_2)$ represents the photoconductivity due to the total intensity $I_1 + I_2$ and $\sigma(I_1)$ the photoconductivity due to the stronger beam, then the lock-in reading in the noninterference condition will be proportional to $\sigma(I_1 + I_2) - \sigma(I_1)$ whereas it will be proportional to $\sigma_g - \sigma(I_1)$ in the interference condition where σ_g is the average photoconductivity given by

$$\sigma_g = \Lambda / \int_0^{\Lambda} \frac{dx}{\sigma(x)}$$

where $\sigma(x)$ is the photoconductivity in interference condition that varies from point to point and is a function of the optical grating period Λ and diffusion length L. The ratio β of the two lock-in readings is given by

$$\beta = \frac{\sigma_g - \sigma(I_1)}{\sigma(I_1 + I_2) - \sigma(I_1)}.$$

An expression for the average conductivity σ_g is obtained below.

The interference of two coherent light beams of intensities I_1 and I_2 falling on the sample produces an intensity pattern given by [76]

$$I(x) = (I_1 + I_2)\left[1 + \gamma_0 \frac{2\sqrt{I_1 I_2}}{I_1 + I_2} cos\left(\frac{2\pi x}{\Lambda}\right)\right]. \qquad (3.1)$$

where $\Lambda = (\lambda/2)sin(\delta/2)$ is the grating period, λ is the wavelength, δ is the angle between the two beams, and x is the coordinate perpendicular to the interference fringes. Also, γ_0 is the factor between zero and unity by which fringe visibility is reduced due to light scattering and mechanical vibrations etc.

The photogenerated carriers in the film follow the following diffusion equation [76]:

$$\overline{D}(N)\frac{d^2N}{dx^2} - R(N) + G = 0, \tag{3.2}$$

where $\overline{D}(N)$ is the effective ambipolar diffusion coefficient given by [76]

$$\overline{D} = \frac{\mu_n^D \overline{D}_p + \mu_p^D \overline{D}_n}{\mu_n^D + \mu_p^D}$$

and $R(N)$ and G are the recombination and generation rates respectively.

The diffusion coefficient $\overline{D}$ and the recombination rate R are dependent on the carrier concentration which makes the Eq. (3.2) nonlinear and, therefore, a general solution for this can not be easily found. However, under the experimental conditions of SSPG ($I_1 \gg I_2$), the carrier concentration N can be written as $N = N_0 + \Delta N(x)$ where $\Delta N(x)$ arises from the weaker beam and is much smaller than N_0. Therefore, the diffusion coefficient $\overline{D}(N)$ can be replaced by its constant equilibrium value $\overline{D}(N_0)$. Similarly, the recombination rate given by $R(N) = \Delta N/\tau(N)$ can be written as $R(N) = \Delta N/\tau(N_0)$ where τ is the mean life time under small signal condition [76]. The generation rate G is also written as $G_0 + \Delta G(x)$ where G_0 arises from the uniform background illumination and $\Delta G(x)$ is due to interference and is much smaller compared to G_0. Substituting $\Delta G(x) = 2\gamma_0\sqrt{I_1 I_2}cos(2\pi x/\Lambda)$ from Eq. (3.1), the Eq. (3.2) simplifies to

$$L^2 \frac{d^2\Delta N(x)}{dx^2} - \Delta N(x) + 2\gamma_0\tau\sqrt{I_1 I_2}\, cos\left(\frac{2\pi x}{\Lambda}\right) = 0, \qquad (3.3)$$

where $L = \sqrt{D\tau}$ is, by definition, the ambipolar diffusion length [110]. $\Delta N(x)$ obtained by solving the Eq. (3.3) is given below

$$\Delta N(x) = \frac{2\gamma_0\tau\sqrt{I_1 I_2}}{[1 + (2\pi L/\Lambda)^2]}\, cos\left(\frac{2\pi x}{\Lambda}\right). \qquad (3.4)$$

Photoconductivity under the interference condition of SSPG can be written as

$$\sigma = \sigma_0 + \Delta\sigma(x) \qquad (3.5)$$

where $\Delta\sigma(x)$ arises from $\Delta G(x)$. Since σ is a function of the number of carriers it is possible to write

$$\Delta\sigma = \frac{d\sigma}{dN}\Delta N = \frac{d\sigma}{dG}\frac{dG}{dN}\Delta N \qquad (3.6)$$

where ΔN is give by Eq. (3.4). Since the photoconductivity has an intensity dependence of the type $\sigma = \sigma_0 G^\gamma$,

$$\frac{d\sigma}{dG} = \frac{\gamma\sigma(x)}{G} \qquad (3.7)$$

and under steady state, we have $R = G$, which gives

$$\frac{dG}{dN} = \frac{dR}{dN} = \frac{1}{\tau}. \qquad (3.8)$$

From Eqs. (3.4), (3.6), (3.7), and (3.8) the Eq. (3.5) can be written as:

$$\sigma(x) = \sigma(I_1 + I_2)\left[1 + Acos\left(\frac{2\pi x}{\Lambda}\right)\right], \qquad (3.9)$$

where $\sigma(I_1 + I_2)$ is the photoconductivity due to uniform illumination of intensity $(I_1 + I_2)$ and

$$A = \frac{2\gamma\gamma_0}{[1 + (2\pi L/\Lambda)^2]} \left(\frac{\sqrt{I_1 I_2}}{I_1 + I_2} \right). \tag{3.10}$$

The average conductivity σ_g, obtained from Eq. (3.9), is

$$\sigma_g = \Lambda / \int_0^\Lambda dx/\sigma(x) = \sigma(I_1 + I_2)\sqrt{1 - A^2}. \tag{3.11}$$

Using Eq. (3.11) the expression of β can be written as

$$\beta = \frac{\sigma(I_1 + I_2)\sqrt{1 - A^2} - \sigma(I_1)}{\sigma(I_1 + I_2) - \sigma(I_1)}. \tag{3.12}$$

Using the power law intensity dependence of photoconductivity in Eq. (3.12), β is found to be

$$\beta = \frac{(I_1 + I_2)^\gamma \sqrt{1 - A^2} - (I_1)^\gamma}{(I_1 + I_2)^\gamma - (I_1)^\gamma}. \tag{3.13}$$

Substituting A from Eq. (3.10) and using the condition $I_1 \gg I_2$, the Eq. (3.13) can be simplified to the following simple expression:

$$\beta = 1 - \frac{2\gamma\gamma_0^2}{[1 + (2\pi L/\Lambda)^2]^2}. \tag{3.14}$$

Therefore, the ambipolar diffusion length L can be obtained from Eq. (3.14) if β, the ratio of photocurrents in interference and noninterference conditions, is measured as a function of the grating period Λ. The exponent γ of intensity dependence of photoconductivity is measured separately whereas the fringe visibility factor γ_0 is taken to be unity in our setup.

CHAPTER

FOUR

Results

The results of the Steady State Photocarrier Grating (SSPG) and Lateral Photovoltage measurements on a-Si:H and a-SiGe:H samples carried out in annealed as well as light soaked states are presented in this chapter.

4.1 The SSPG Measurement on a-Si:H

The Fig 4.1 shows the plots of the ratio 'β' of photocurrents in interference and noninterference conditions (see Chapter. 3) as function of the grating period 'Λ' for the a-Si:H film s0. The data taken in the annealed ($T_A = 470K$, 2 hours) state is shown by open circles whereas that taken in the light soaked (LS) state by filled circles. The solid lines

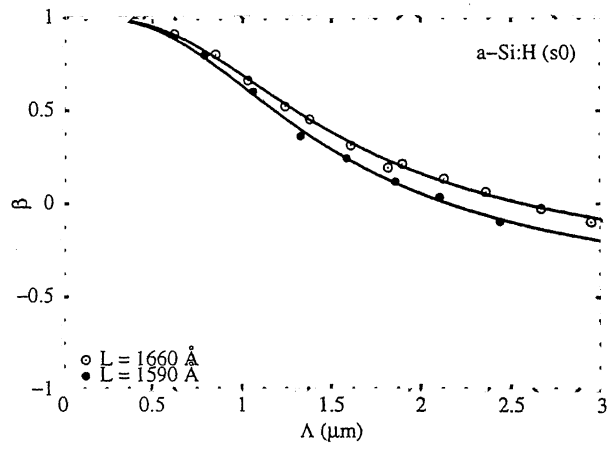

Figure 4.1: β vs grating period Λ of the SSPG measurement on a-Si:H (s0) in annealed (o) and light soaked (•) state. The lines are the fit to the Eq.(3.14) and the hole diffusion length L which gives the best fit are indicated.

in these figures are obtained by the least square fit of Eq. (3.14) to the experimental data. A good fit is obtained for $L = 1660 \pm 60$Å in the annealed state of the sample and in the LS state a good fit is obtained for $L = 1570 \pm 60$Å.

The plot of 'Λ' vs 'β' for another a-Si:H sample (s1) is shown in the Fig. 4.2. The measurement is carried out in the annealed and LS state for this sample as well. A fit of the data points, to Eq. (3.14) gives the minority carrier (hole) diffusion length $L = 830 \pm 90$Å and $L = 330 \pm 40$Å in annealed and light soaked states respectively.

The effect of light soaking on s0 (Fig. 4.1) is small compared to

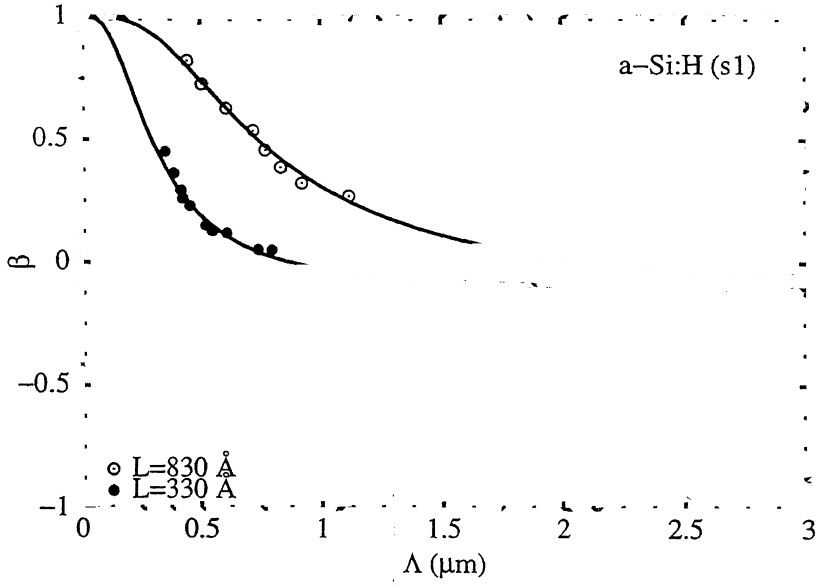

Figure 4.2: β vs grating period Λ of the SSPG measurement on a-Si:H (s1) in annealed (o) and light soaked (•)state. The lines drawn are the fit to the Eq. (3.14).

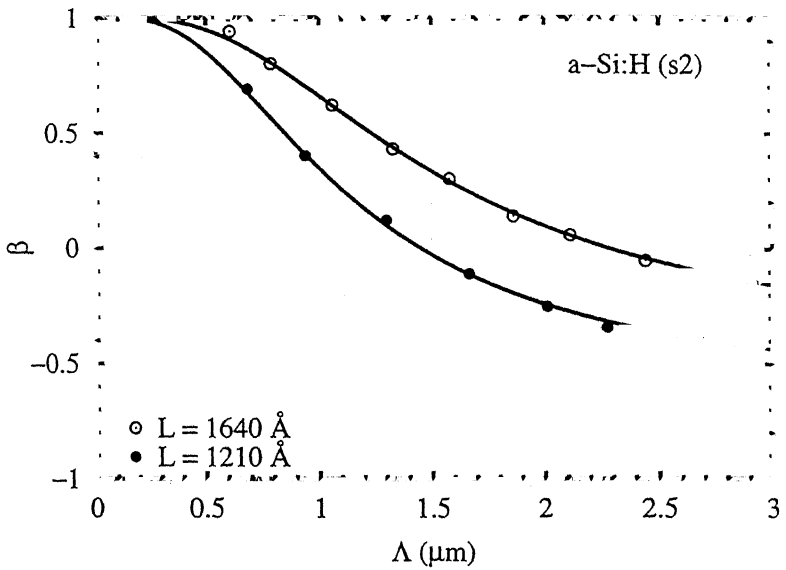

Figure 4.3: β vs grating period Λ of the SSPG measurement on a-Si:H (s2) in annealed (o) and light soaked state (•). The lines drawn are the fit to the Eq. (3.14).

that on s1 (Fig 4.2). The sample s0 is exposed to light from a 50W (15mW/cm^2) tungsten halogen for 4 hours, whereas s1 is light soaked for 24 hours using a 360W (100mW/cm^2) tungsten halogen lamp. A water filled beaker and an IR reflector are used to prevent the heating of the samples during LS. This decrease in ambipolar diffusion length upon LS is qualitatively, in good agreement with the published results [10, 76–78].

4.2 The SSPG Measurement on a-SiGe:H

We have measured L for a set of samples prepared under identical deposition conditions with different germanium concentrations. The Ge [GeH_4/(SiH_4+GeH_4)] concentration was chosen to be 0%, 10% and 20% for the three samples. The Fig. 4.4 shows the results of SSPG measurements on the sample with 10% Ge (s3). As before, the filled circles denote the LS state whereas the open circles represent the annealed state and the smooth curve is obtained as described earlier. The values of L in the annealed and the LS state are 740 ± 90Å and 580 ± 70Å respectively.

Similarly, the results obtained on the sample (s4) with 20% Ge are shown in the Fig. 4.5 and the values of L in annealed and LS states for this sample are 284 ± 40Å and 207 ± 30Å respectively.

The variation of L, both in annealed and LS state, as a function of

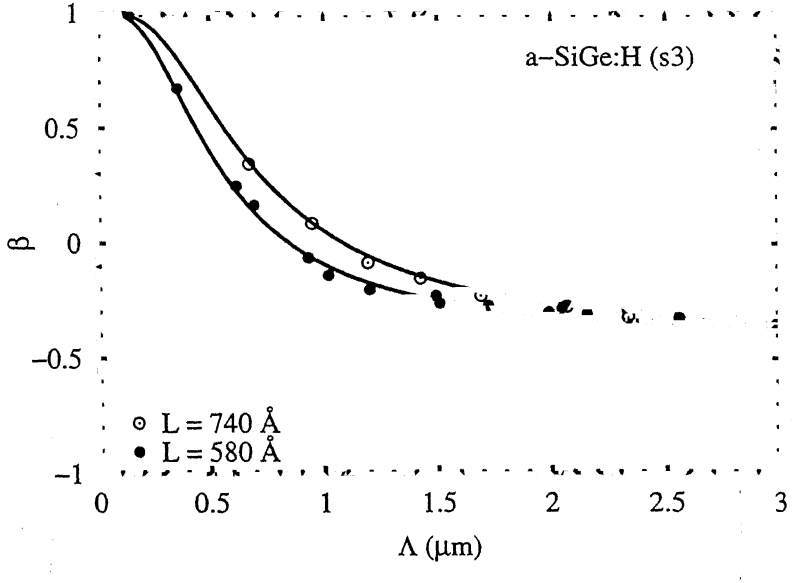

Figure 4.4: β vs grating period Λ of the SSPG measurement on a-SiGe:H (s3) having 10% Ge [GeH_4/(SiH_4+GeH_4)] in annealed (o)and light soaked state (•). The lines drawn are the fit to the Eq. (3.14).

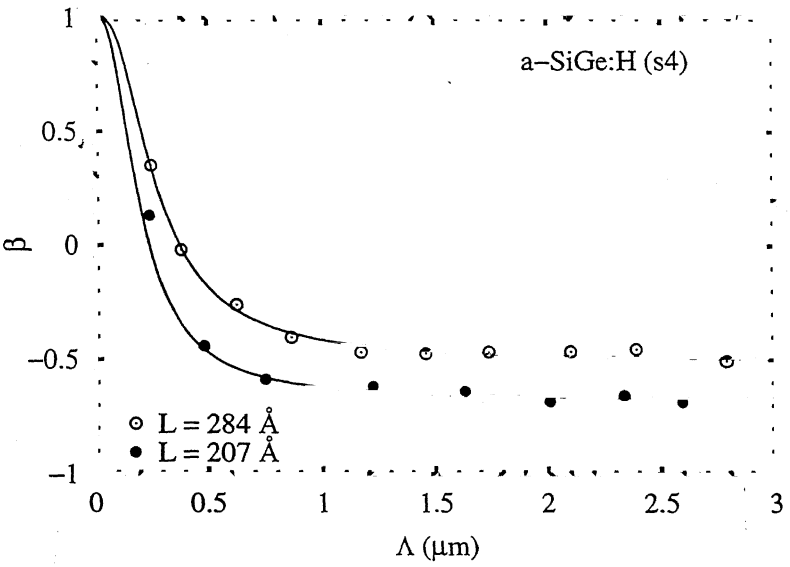

Figure 4.5: β vs grating period Λ of the SSPG measurement on a-SiGe:H (s4) having 20% Ge [GeH_4/(SiH_4+GeH_4)] in annealed (o) and light soaked state (•). The lines drawn are the fit to the Eq. (3.14).

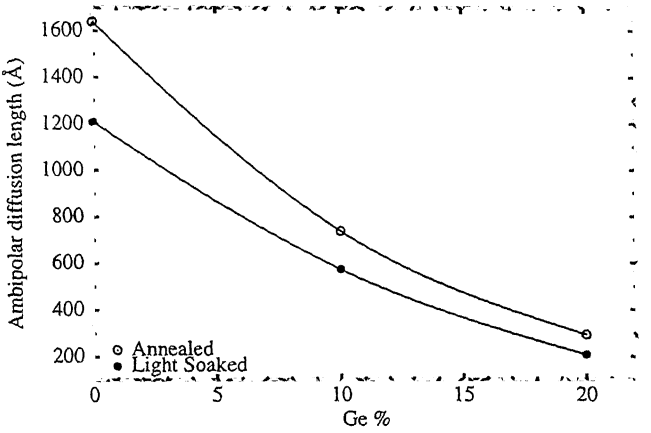

Figure 4.6: The variation of L with increasing Ge [GeH_4/ (SiH_4 + GeH_4)] content. The lines drawn are the guide to the eye.

the Ge content is shown in the Fig. 4.6. The L in annealed as well as LS state decreases with increasing Ge concentration.

The two a-Si:H samples s1 and s2 are prepared under in different systems under somewhat different conditions. The density of states of the sample s1 is higher than the sample s2. The Figs. 4.2 and 4.3 it is clear that the ambipolar diffusion length of s1 is smaller compared to that of s2 and it reduces upon light soaking in both the samples.

4.3 Lateral Photovoltage Measurement

The LPV measurements are carried out as described in the Sec. 2.4. Fig. 4.7 shows the plot of LPV as a function of the position of the laser spot measured at different temperatures on sample s1 in the annealed state. The position of the laser spot is measured with respect to the center of the sample. As the laser spot is moved from one end to the other, the LPV decreases (in magnitude) and becomes zero at the center of the film. When the laser is moved further away, towards the other end of the sample, there is a sign reversal in LPV and its magnitude increases as we approach the other end. Also, the magnitudes of LPV at equal distances on the two sides of the center are nearly equal showing the symmetric nature of LPV. Further, the electrode closer to the light spot is found to be always negative.

Results of LPV measurement on another a-Si:H (s2) are shown in Fig. 4.8. For this sample also, the LPV decreases in magnitude while moving towards the center and again increases with a sign reversal as the other end is reached. It can be seen from this figure that the position dependence of LPV for this sample is qualitatively similar to that of previously described sample (s1). However, the magnitude of LPV at the same distance from center for s2 is smaller compared to that measured on s1.

LPV measured on a-SiGe:H (s3) with 10% Ge is shown in Fig. 4.9 and has a maximum value of about 8mV in annealed state and about

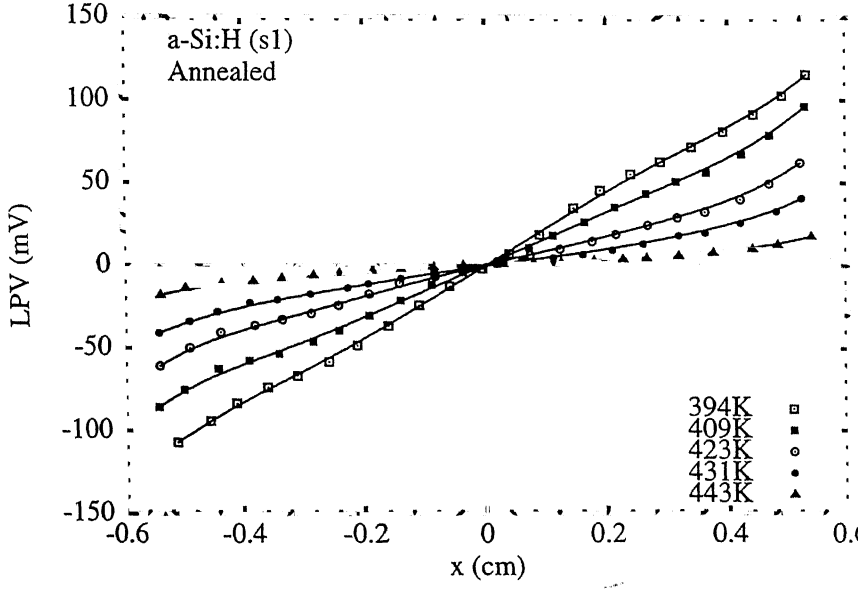

Figure 4.7: ***LPV*** as a function of the position of the center of illumination measured at different temperatures on a-Si:H (s1) in annealed state.

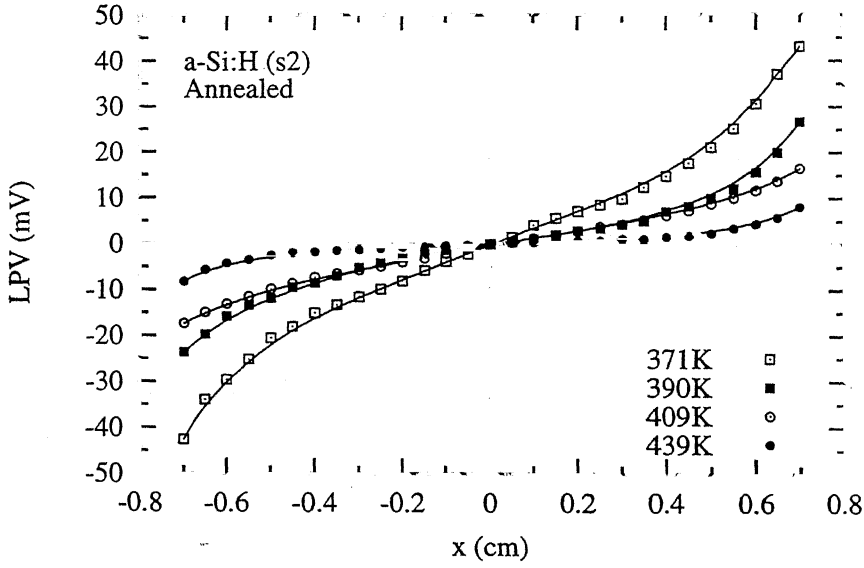

Figure 4.8: *LPV* on a-Si:H (s2) in annealed state as a function of the position of the illuminated spot for different measurement temperatures.

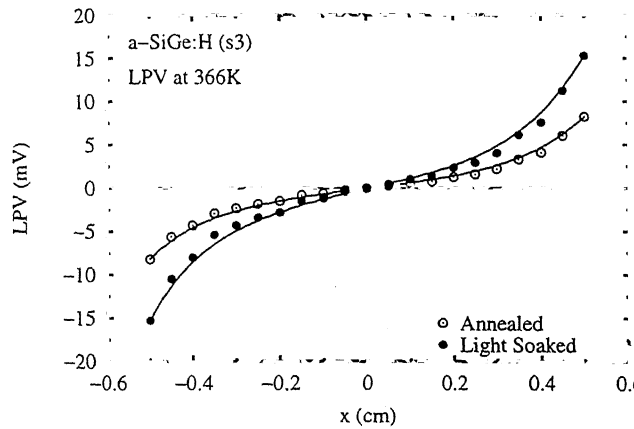

Figure 4.9: LPV measured at 366K on a-SiGe:H (s3) in annealed and light soaked states as a function of the position of the illuminated spot.

15mV in the LS state. It is also qualitatively similar to the results of LPV on a-Si:H samples (s1 and s2) as described earlier. LPV on the a-SiGe:H sample with higher Ge content was very small and could not be measured accurately as a function of position of the light spot. The LPV results are summarized in the Table 4.1.

4.3.1 Temperature dependence of LPV

Figs. 4.7 and 4.8 show that LPV on s1 and s2 decreases with increasing measurement temperature. To obtain the temperature dependence, LPV is measured at different temperatures while keeping the laser spot at a fixed position x. LPV decreases as the temperature is raised

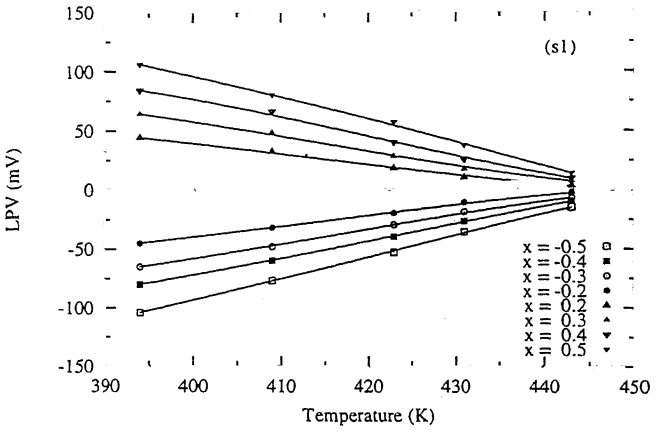

Figure 4.10: Temperatures dependence of LPV on a-Si:H (s1), measured while keeping the laser fixed at different positions.

from 395K to 445K. For each value of x, the temperature dependence of LPV follows the same pattern as shown in Figs. 4.10 and 4.11 for samples s1 and s2 respectively.

4.3.2 Effect of Light Soaking on LPV

LPV measured at 394K after light soaking (LS) the sample s1 is plotted in Fig. 4.12. For the sake of comparison the LPV measured in the annealed state is also plotted on the same figure. It is easy to see that the LPV increase after LS. However, there is no qualitative change in its position dependence, i.e. it undergoes a sign reversal at the center

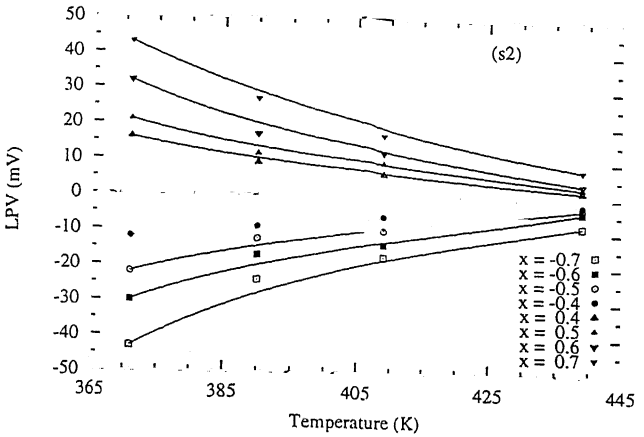

Figure 4.11: Temperatures dependence of LPV on a-Si:H (s2), measured while keeping the laser fixed at different positions.

and increases in magnitude as the laser spot is moved away from the center.

Figs. 4.13 and 4.14 show the LPV measured at 409K and 431K respectively and is easy to see that the LPV after LS is always higher than that in the annealed state. Also, as the temperature goes up, the LPV decreases as in the case of annealed state.

Figs. 4.15 and 4.16 show the plot of LPV before and after LS, measured at 371K and 390K on the other a-Si:H sample (s2). As in the case of s1, the LPV increases upon light soaking for this sample as well. The position dependence of LPV remains qualitatively similar

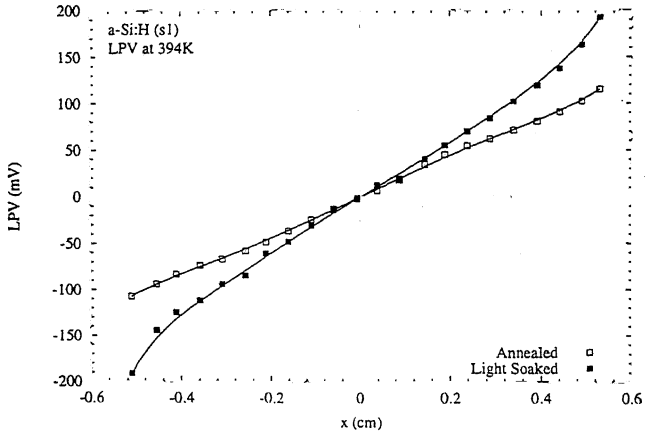

Figure 4.12: *LPV* measured at a 394K before and after LS on a-Si:H (s1) for different positions of the laser.

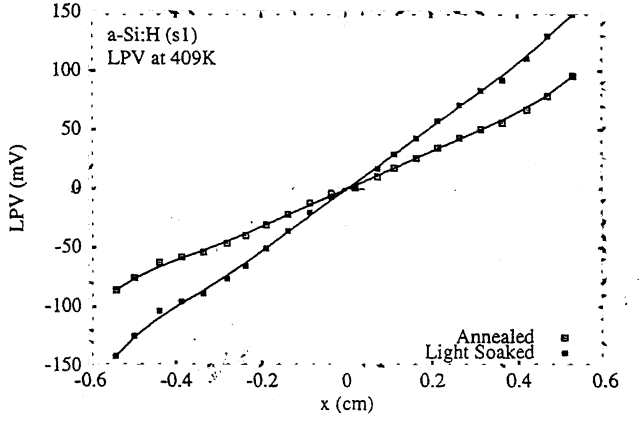

Figure 4.13: *LPV* measured at a 409K before and after LS on a-Si:H (s1) for different positions of the laser.

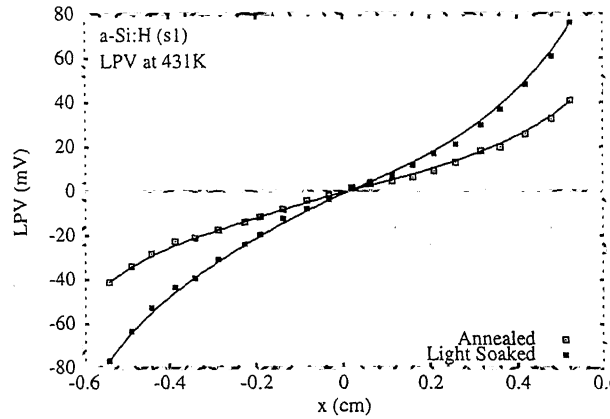

Figure 4.14: *LPV* measured at a 431K before and after LS on a-Si:H (s1) for different positions of the laser.

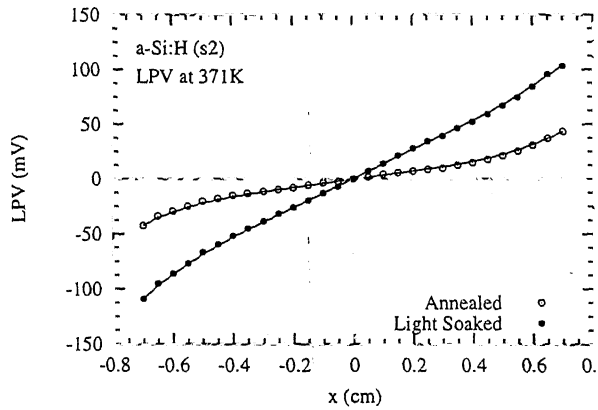

Figure 4.15: *LPV* measured at a 371K before and after LS on a-Si:H (s2) for different positions of the laser.

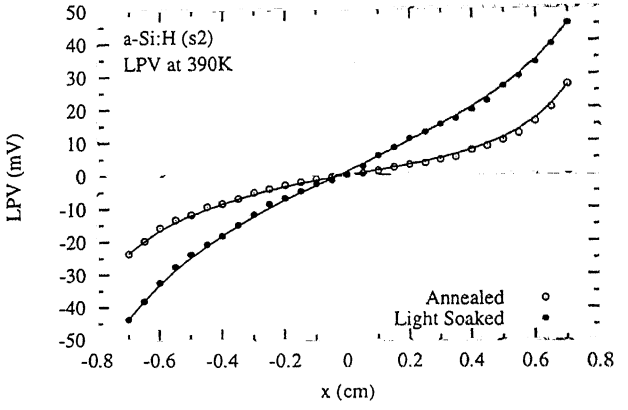

Figure 4.16: LPV measured at a 390K before and after LS on a-Si:H (s2) for different positions of the laser.

to that of the annealed state, albeit, with a higher magnitude. Qualitatively similar results are obtained for a-SiGe:H sample (Fig. 4.9).

This rise in LPV on LS is a very surprising result as one would have expected it to go down vis-à-vis the decrease in the L of the carriers upon LS as shown in SSPG measurement (see Fig. 4.2 and Fig. 4.3).

4.4 Summary

The results of both L and LPV measurements are summarized in the Table 4.1. The ambipolar diffusion length reduces upon light soaking for the a-Si:H samples. Effect of LS is similar on the a-SiGe:H samples i.e. it reduces the ambipolar diffusion length in these samples as well.

Table 4.1: LPV at 5mm from the center and diffusion lengths at 300K in annealed and light soaked (LS) states.

Sample	L(Å) (Annealed)	L(Å) (LS)	LPV (mV) (Annealed)	LPV (mV) (LS)
s0 (a-Si:H)	1660 ± 60	1570 ± 60	—	—
s1 (a-Si:H)	830 ± 90	330 ± 40	115 (394K)	190 (394K)
s2 (a-Si:H)	1640 ± 20	1210 ± 90	27 (390K)	45 (390K)
s3 (a-SiGe:H)	740 ± 90	580 ± 70	8 (366K)	15 (366K)
s4 (a-SiGe:H)	284 ± 40	207 ± 30	—	—

The incorporation of Ge in the samples reduces the ambipolar diffusion length drastically as the concentration of germanium is increased in the samples from 0% to 10%. There is a further reduction in L when Ge content is raised from 10% to 20%. Moreover, the samples with still higher concentration of Ge did not have any photoconductivity and no SSPG measurements were possible.

LPV is measured on samples s1, s2, s3 and s4 and is found to be qualitatively similar for all the samples. It is much smaller on a-SiGe:H samples compared to that measured on the samples without Ge. LPV on the sample with 20% Ge was very small and could not be measured accurately as a function of position of laser spot and is not reported here.

CHAPTER

FIVE

Discussion

5.1 Analysis of Lateral Photovoltage

The results of SSPG and LPV measurements on a-Si:H and a-SiGe:H samples have been presented in the previous chapter. The main features which need to be explained are

- The shape and magnitude of LPV and
- The change in LPV upon light soaking.

Let us first see, if these can be understood in a rigid band model, in which the conduction and valence band edges remain fixed in space

and the photoexcited electrons and holes diffuse with different diffusion lengths.

5.1.1 Carrier Diffusion during LPV measurement

The LPV measurements presents a case of departure from equilibrium of the carrier distribution in semiconductors. The carrier density in the illuminated region is much higher compared to the nearby dark region. This leads to diffusion of photocarriers from the illuminated to the dark regions. This diffusion of carriers is governed by the continuity and Poisson equations [110] which are presented here, for the sake of simplicity, let us consider one dimensional case.

$$G - R + \frac{\partial}{\partial x}\left(n(x)\mu_n E(x) + D_e \frac{\partial n(x)}{\partial x}\right) = 0, \tag{5.1}$$

$$G - R - \frac{\partial}{\partial x}\left(p(x)\mu_p E(x) - D_h \frac{\partial p(x)}{\partial x}\right) = 0, \tag{5.2}$$

and

$$\frac{\partial E(x)}{\partial x} = \left(\frac{e}{\epsilon}\right)(p(x) - n(x)). \tag{5.3}$$

Here G is the generation rate of photocarriers, D_e and D_h are the diffusion coefficients of electrons and holes respectively, R the recombination rate, ϵ the permittivity of a-Si:H and $n(x)$ and $p(x)$ are the total number of electrons and holes at a distance x from the point of illumination x_0 in the steady state. More explicitly, $n(x) = n_0 + \delta n(x)$

and $p(x) = p_0 + \delta p(x)$, where n_0 and p_0, are the carrier concentrations in dark (independent of x) and $\delta n(x)$ and $\delta p(x)$ are the excess photogenerated carriers and depend on x. The terms inside the parentheses in Eqs. (5.1) and (5.2) represent the gradients of the drift and diffusion components of the current density respectively. Here E is the internal field which is related to the LPV by the following relation

$$E = -\frac{\partial V}{\partial x}, \tag{5.4}$$

where V is the measured LPV. These equations are also subject to the charge neutrality condition.

This set of equation should be solved with appropriate boundary conditions to obtain the charge distribution which, in turn, can be used to get the LPV. The diffusion equations are, however, nonlinear due to a probable dependence of diffusion coefficient and the recombination rate on the carrier concentrations. A small signal approximation, as in the case of SSPG (see Chapter. 3), is not applicable here because the departure from equilibrium is very large in the case of LPV compared to that in SSPG. In general, an exact solution of these equations is difficult to obtain and is usually found under various approximation schemes [110]. These approximations depend on the conditions under which charge transport takes place in the system. For the present case an exact solution is not necessary and it is possible to estimate LPV by assuming a physically acceptable charge profile for the photocarriers, as described below.

5.1.2 Estimation of Lateral Photovoltage

For a one dimensional case, we assume that the illumination of the sample produces linear charge distribution of photocarriers having a width $2W$. Further, we assume that the carriers diffuse to the dark regions from sides of the linear charge profile giving exponential tails at both the ends. The exponential tail have decay lengths equal to the diffusion lengths of the respective carriers. The central part of the charge profiles have the widths (with constant linear charge density ρ_0) $2w_e$ and $2w_h$ for electrons and holes respectively. If the diffusion lengths of electrons and holes are L_e and L_h respectively, then the charge profiles of photocarriers in a one dimensional case are given by the following:

$$\rho_{e,h}(x) = \rho_0 \exp\left(\frac{w_{e,h} + x}{L_{e,h}}\right) \quad -\infty \leq x \leq -w_{e,h}, \tag{5.5}$$

$$\rho_{e,h}(x) = \rho_0 \qquad -w_{e,h} \leq x \leq w_{e,h}, \tag{5.6}$$

$$\rho_{e,h}(x) = \rho_0 \exp\left(\frac{w_{e,h} - x}{L_{e,h}}\right) \quad w_{e,h} \leq x \leq \infty. \tag{5.7}$$

If there are N charges in the profile, we have $\rho_0 = N/2W$ and from the charge neutrality condition $w_{e,h} = W - L_{e,h}$.

The potential at a point at a distance d from this charge profile can

be written in terms of multipole expansion

$$V = \frac{1}{4\pi\epsilon_0\epsilon} \sum_{n=0}^{n=\infty} \frac{1}{d^{(n+1)}} \int_{-\infty}^{\infty} x^n(\rho_h(x) - \rho_e(x))dx. \tag{5.8}$$

Because of the charge neutrality, the monopole term ($n = 0$) is zero and the symmetric charge profiles $\rho_{e,h}(x)$ make the dipole term vanish. Thus the largest nonzero contribution to potential comes from the quadrupole term ($n = 2$) of the multipole expansion which gives

$$V = \frac{1}{4\pi\epsilon_0\epsilon} \left\{ \frac{1}{d^3} \int_{-\infty}^{\infty} x^2(\rho_h(x) - \rho_e(x))dx \right\}. \tag{5.9}$$

Using the charge profiles given by Eqs. (5.5), (5.6) and (5.7), we have

$$V = \frac{Ne}{4\pi\epsilon_0\epsilon d^3} \left\{ (L_h^2 - L_e^2) + \frac{2(L_h^3 - L_e^3)}{3W} \right\}. \tag{5.10}$$

Under experimental conditions we have $W >> L_{e,h}$, the second term in the parentheses can be neglected. This simplifies the Eq. (5.10) for potential to

$$V = \frac{1}{4\pi\epsilon_0\epsilon} \frac{Ne(L_h^2 - L_e^2)}{d^3}. \tag{5.11}$$

Hence, the expression for LPV, which is the potential difference between the two electrodes is

$$LPV = \frac{Ne(L_h^2 - L_e^2)}{4\pi\epsilon_0\epsilon} \left\{ \frac{1}{(s+x)^3} - \frac{1}{(s-x)^3} \right\}, \tag{5.12}$$

where $2s$ is the separation between the electrodes and x the distance of the center of light spot from the center of the film. It is clear from the Eq. (5.12) that LPV is zero when the illumination is at the center ($x = 0$) and it identically reduces to zero at every position of illumination if $L_e = L_h$. This is akin to condition for the existence of Dember voltage [75]. Taking $L_e = 10L_h = 10L$, we get

$$LPV = \frac{99L^2Ne}{4\pi\epsilon_0\epsilon}\left\{\frac{1}{(s-x)^3} - \frac{1}{(s+x)^3}\right\} \tag{5.13}$$

For a typical calculation we take $L = 0.1\mu m$, $s = 9mm$ (half the electrode separation), $\epsilon = 12$ for a-Si:H; LPV can be estimated from Eq. (5.13) if we know the number of charge carriers N in the equilibrium. For the intensity of the laser used in LPV experiment, we have $\sigma_{ph}/\sigma_d = 5 \times 10^5$ (for sample s1). This gives a total of about 10^7 photogenerated charges in the volume of the illuminated region (a circular spot of about 3mm diameter on a $1\mu m$ thick sample), in the extended states. In addition, if the density of localized states is taken to be constant ($10^{17}cm^{-3}eV^{-1}$) and occupied within the quasi Fermi levels, the number of localized charges are about 4×10^{11}, taking the splitting to be 0.4 eV. For the largest possible LPV we assume that the localized charges have the same profiles as the charges in the extended states and take $N = 4 \times 10^{11}$.

The calculated LPV using these numbers and above assumption is shown in Fig 5.1. A comparison with Figs 4.7 and 4.8 shows that although their shapes are similar, the calculated LPV is much smaller

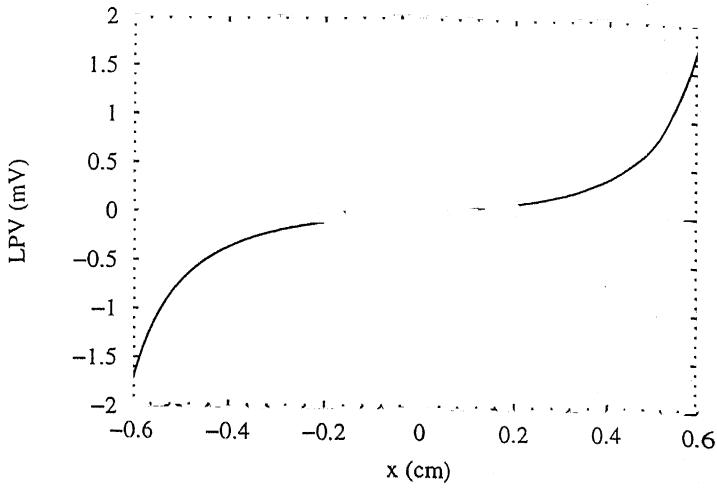

Figure 5.1: Lateral photovoltage as calculated using Eq. (5.13) with $L_e = 1\mu m, L_h = L = 0.1\mu m$. Other parameters are given in Sec 5.1.2.

than the experimental values. For sample s1 in annealed state, the measured LPV at $x = 0.5cm$ is about 2 orders of magnitude higher compared to the calculated LPV. For sample s2, the measured LPV is larger by a factor of 25. Therefore, these simple considerations can not explain our results satisfactorily.

Another puzzle relates to the observed increase in LPV upon light soaking. Our measurements (Table 4.1) as well as those in the literature [10, 76–78] indicate that the diffusion length (L) of carriers decreases after light soaking. Thus, we expect LPV to decrease after LS

[see Eq. (5.13)]. The observed opposite trend shows that the present considerations are inadequate to explain our results.

Therefore, we conclude that although the rigid band model, in which the photogenerated electrons and holes have different diffusion lengths can qualitatively explain the shape of the LPV vs x curve observed experimentally, the magnitude of the observed LPV is much larger than the calculated LPV. The discrepancy is as large as about 2 orders of magnitudes in some cases and can not be resolved, even if we take the most favorable values of the unknown parameters. In order to explain the observed magnitude, either N or L (or both) in Eq. (5.13) will have to be larger. The conventional approch not only fails to explain the large magnitudes, it cannot account for the increase in LPV after light soaking. Thus, an alternate model is necessary to account for the seemingly anomalous behaviour of LPV.

So far the heterogeneities present in a-Si:H and alloys, have not been taken into account. We believe that the presence of heterogeneities might be responsible for this large LPV. In the next section, we discuss how the potential fluctuations arising from these heterogeneties might explain our results.

5.2 Potential fluctuations in a-Si:H and alloys

It is well accepted that heterogeneities are present even in the best quality a-Si:H and a-SiGe:H films [21, 22, 111] and give rise to potential fluctuations [15]. Potential fluctuations have profound effect on the electronic properties of hydrogenated amorphous silicon and its alloys. These have been invoked to explain a number of observations such as the disagreement between the values of density of localised states obtained by the optical absorption and the electrical measurements [18], difference in thermopower and conductivity activation energies [24] and persistent photoconductivity in a-Si:H *p-n* multilayers [112]. Howard and Street [27] explain the rapid drop in drift mobilities in compensated a-Si:H with increasing compensation as arising from the potential fluctuations. The transport properties of a-Si:H prepared by hot wire technique [113] and the influence of light-induced degradation on the extended state mobility in a-Si:H by Schmidt et al [114] are also explained using the concept of potential fluctuations. Potential fluctuations have also been used to explain the transport properties of hydrogenated amorphous silicon carbide films [28] and the light induced degradation in undoped hydrogenated amorphous silicon [29–32]. The difference in the optical absorption coefficient in a-Si:H measured by two methods, viz, photothermal deflection spectroscopy (PDS)

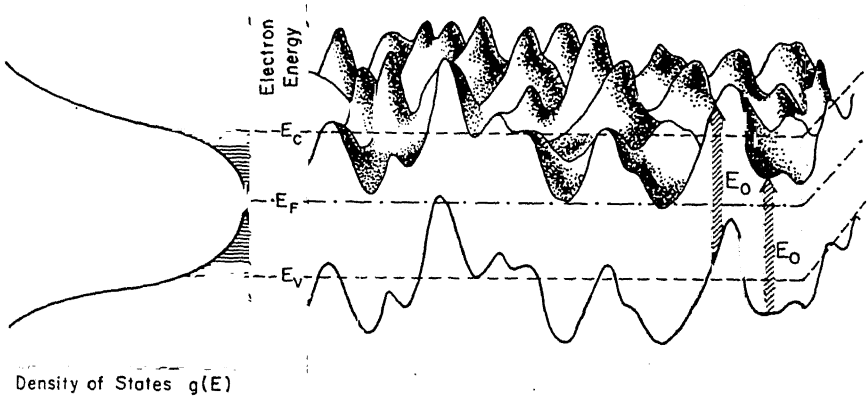

Figure 5.2: Long range potential fluctuations as might be present in a-Si:H. This figure shows only the electrostatic part of the potential fluctuations where the band gap does not vary from point-to-point in the material. The elastic fluctuation which involves the variation of band gap E_0 has been omitted for clarity. After ref. 18.

and Constant Photocurrent Method (CPM), has been attributed partly to the presence of potential fluctuations [34].

The presence of potential fluctuations in a-Si:H and a-SiGe:H films results in spatial variation in the conduction (E_c) and valence (E_v) bands as shown in Fig. 5.2. Only symmetric part of the potential fluctuations is shown here for the sake of clarity.

5.3 Potential Fluctuation Model for LPV

In the presence of potential fluctuations, the photogenerated electrons and holes move in the presence of the internal fields and electrons and

holes get separated spatially. Their spatial separation due to internal fields arising from potential fluctuations may result in the carrier profiles quite different from that envisaged from the diffusion of carriers in the absence of potential fluctuations. Also, this may reduce their recombination probability resulting in a larger L. In this connection, we note that in a-Si:H, the diffusion length (L) measured by SSPG is reported to decrease with the increasing intensity of light [77]. Since the effect of light is to reduce the potential fluctuations that might be present in the material, this is understandable. Further, as already mentioned in the Sec. 2.3.1, the SSPG measurements are performed in presence of a bias light and are therefore likely to underestimate L.

Since the LPV measurements reported in Chapter 4 are done in the absence of any bias light, it is not correct to use the L measured in the presence of bias light in Eq. (5.13) to calculate LPV. Since the bias light is expected to reduce the potential fluctuations [115], LPV is expected to be smaller when measured in the presence of bias light. We indeed find that the value of LPV is much smaller with the bias light than that measured without bias light (See Fig 5.3). The LPV measured with bias light is comparable to the calculated value (See Fig. 5.1). This supports the potential fluctuations model for LPV.

Now we show that in this model, N is expected to have a larger value than that estimated from the rigid band model(section 5.1.2). The increase of LPV after light soaking can also be explained on the basis of proposed potential fluctuation model.

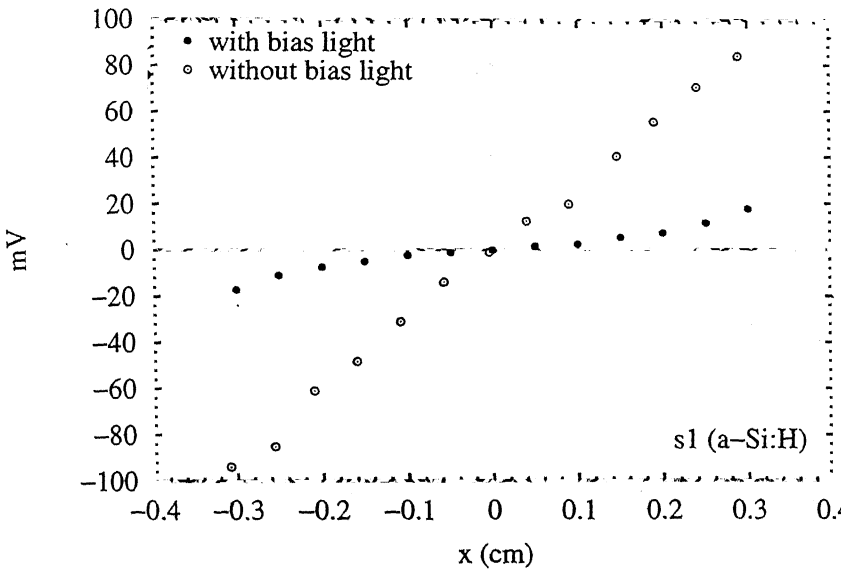

Figure 5.3: LPV, measured in the light soaked state of a-Si:H (s1), in the presence of a strong bias light is plotted after multiplying by 10. For comparison LPV on the same sample, measured without bias light is also shown. LPV with bias light is much smaller than that without the bias light.

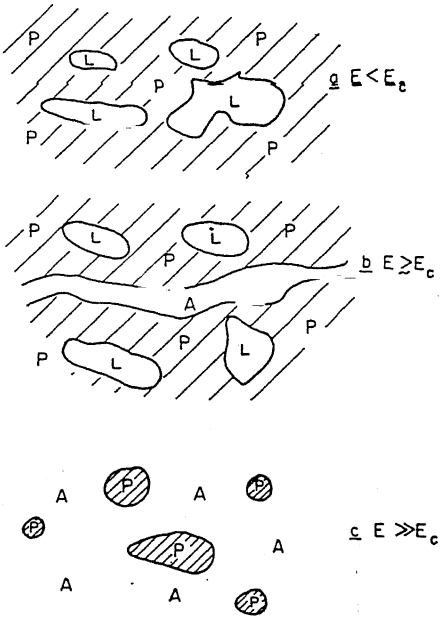

Figure 5.4: (a) For energy below the percolation threshold E_c there are localized allowed regions **L** embedded in prohibited space P as seen in the top of the Fig. (b) When $E = E_c$ the first allowed paths (channeling states) **A** appear and connect one side of the material with the other. They coexist with the allowed islands **L** as shown in the middle part. (c) At high energies $E \gg E_c$ the prohibited regions have shrunk to isolated islands. After ref. 18.

It is to be noted that only those charges which are above the percolation threshold give rise to photocurrent; however, N in Eq. (5.13) includes all charges i.e., those in the localized states also, since these also contribute to LPV. Though, we have taken into account the localized charges in the calculation of LPV, their estimate was based on the assumption of rigid band picture in which all the states above the conduction band edge are believed to be extended states. However, in the potential fluctuation model, there are regions of localized states, marked by letter **L** in Fig. 5.4, that coexist with the extended (channeling) states marked by **A**. In particular the first extended states close to E_c and E_v, the percolation edges, are the channeling states which occupy a small fraction of space and coexist with many localized regions **L** [18]. The contribution to N from the charges in the localized regions above the percolation edge can be quite large as the channeling states occupy only a small fraction of space in the material. Therefore, we expect larger potential fluctuations to give rise to larger LPV.

It has been reported by several workers [32, 116, 117] that the effect of light soaking is to increase the potential fluctuations. Thus, the observed increase in LPV after LS (see Table 4.1) for both the samples s1 and s2 is as expected. Similar comments can be made about the a-SiGe:H alloy sample also. However, it does not seem fair to compare a-SiGe:H sample with a-Si:H samples (with no Ge) as their band gaps and other parameters are quite different.

LPV decreases with increasing temperature and has temperature

dependence as shown in Figs. 4.10 and 4.11 for samples s1 and s2. The temperature dependence can also be qualitatively understood. As the measurement temperature is raised, the charges in the localized regions above percolation threshold have higher recombination probability which, in turn, may lead to smaller L as well as decreased N resulting in a smaller LPV as observed.

5.4 Effect of Band Bending on LPV

So far we have considered only the role of potential fluctuations on LPV. However, both a-Si:H and a-SiGe:H films may have band bending at the surfaces and these might also contribute to the magnitude of LPV. If the bands at the top and bottom surfaces are bent in the appropriate directions, they can help in separating the photogenerated carriers so that they do not recombine easily. This may result in larger diffusion lengths L and therefore large LPV. In the absence of any definite information about the surface band bending, it is difficult to estimate the extent to which the band bending does affect the carrier diffusion by separating them physically to different regions. However, it can be said that the band bending are presented with different scenarios in SSPG and LPV and might play different roles.

From the above discussion, it is clear that the large magnitude of LPV, which appears to be anomalous and is difficult to account for by

the diffusion lengths considerations in a rigid band model, can be explained by taking the potential fluctuations into account. The potential fluctuations are known to influence the carrier transport in amorphous silicon. Here, we have seen how these potential fluctuations might influence the diffusion length L and number of charge carriers that should be taken into account for estimating LPV. Further, these considerations also explain the observed decrease in LPV with increasing temperatures and an increase in it after light soaking quite well.

CHAPTER

SIX

Summary and Conclusions

Hydrogenated amorphous silicon (a-Si:H) and amorphous silicon germanium (a-SiGe:H) films have been prepared by r.f. glow discharge technique and characterized structurally, electrically and optically. X-ray diffraction and electron diffraction show that these samples have amorphous structure. Conductivity (σ), Photoconductivity, and optical gap are found to be similar to those reported in the literature for good quality a-Si:H. The density of states measurements by constant photocurrent method (CPM) indicate that these samples are of device quality.

We have used the Steady State Photocarrier Grating (SSPG) technique to measure the ambipolar (holes) diffusion length (L) in a-Si:H

and a-SiGe:H samples. Table 4.1 summarizes the results. Moreover, we note that L decrease with incorporation of germanium in the films. This decrease in L with the Ge incorporation is attributed to the increase in the density of localized states [118–120] and is also supported by our CPM measurements Table 2.1. Moreover, for all the samples studied the diffusion length decreases with light soaking as the density of localized states rises upon LS. These findings are as expected and are in agreement with the published results [76–78].

A large open circuit voltage develops between two coplanar electrodes when the samples are illuminated by a laser spot between them. This Lateral photovoltage (LPV) depends on the position of the laser spot and decreases as the measurement temperature increases. Although light soaking decrease L, we find that contrary to our expectations, LPV increases.

The existence of LPV can be understood in terms of photocarrier diffusion. Since the electrons and holes have different diffusion lengths, they diffuse and give different charge profiles. If the two electrodes are at unequal distances from the illuminated spot, they will be at different electrostatic potentials. Based on this, an estimate of LPV is made as described in Chapter 5. We find that $LPV \propto L^2N$, where L is the hole diffusion length and N the total number of photogenerated carriers. As the diffusion length is found to reduce upon light soaking (LS), the increase in LPV after LS is counterintuitive. Moreover, the magnitude

of LPV measured in all cases is found to be much larger than calculated using the measured L and the number of available photocarriers (N) estimated from photoconductivity.

Thus, LPV is an interesting phenomenon from the physics point of view. Moreover, the observation of large LPV (nearly 100mV in some cases) shows that this simple device structure can be used as a large area position sensitive detector.

We have shown that LPV can not be explained using the rigid band model and find that heterogieneities can explain our results. The heterogeneities may arise from nonuniform distribution of hydrogen and variation in Si, Ge concentration from point to point in the a-SiGe:H films. They are expected to give rise to potential fluctuations as explained in Sec. 1.2 [18]. In our model, the effect of these potential fluctuations is two fold. The electrons and holes may get separated spatially in the presence of the potential fluctuations. This tends to reduce their recombination probability and might result in an increase of L. One might argue that since we are using the value of L which we actually measured by SSPG; this has to correct. However, we note that SSPG measures L in the presence of bias light since one of the beams is much stronger than the other as explained in the Sec. 2.3.1. Since we cannot measure L without disturbing potential fluctuations by bias light, we measured LPV in the presence of bias light, instead. If bias reduces L, LPV should also be reduced. This is indeed observed (See Fig. 5.3). This explanation of LPV in terms of potential fluctuations

agrees with the observation of Weiser and Ritter [77], who found that the value of L measured by SSPG decreases, as the light intensity increases. Further, we note that SSPG measurements are always done in the presence of light, and therefore, expected to give a smaller L than its value in dark.

Further, in the potential fluctuation model, there are channel states which conduct and there are large regions of carrier occumulation which do not participate in conduction. Therefore, photoconductivity takes into account only the charges in the channel states, whereas, all charges including those outside the channel also contribute to LPV. Thus the value of N used in calculaing LPV is likely to be underestimated by a large amount. Hence, larger potential fluctuations are likely to give large LPV since both N and L in Eq. (5.13) are expected to have higher values than obtained from the rigid band model.

The increase in LPV after light soaking in all the samples can also be explained by this model. Since light soaking increases the potential fluctuations [116, 117], the increase in LPV is understandable.

Thus we can explain all our data by the potential fluctuation model. A more quantitative analysis is not possible at this stage. It is, however, clear that more heterogeneous sample should show larger LPV since the potential fluctuations are more. This is an interesting observation which could be useful in comparing quality of samples prepared under different conditions. This requires more experimentation.

Other factors like band bending at the surfaces might also contribute to large magnitude of LPV by physically separating the carriers, whereby decreasing their recombination in the similar way as the potential fluctuations.

Scope of future work

It is shown that the LPV can be understood in terms of potential fluctuations which arise out of heterogeneities in these materials. In order to further understand the physics of LPV the first step would be a simultaneous measurement of LPV and potential fluctuations in the same sample. The potential fluctuations can be estimated by conductivity and thermopower measurement [24, 33]. LPV measurements coupled with conductivity and thermopower on a set of samples prepared under different preparation conditions and having different hydrogen concentrations may help in correlating LPV with potential fluctuations in a quantitative manner.

Moreover, wavelength dependence of LPV might help in understanding the role of surfaces as well as the various localized states in the gap. As the absorption coefficient increases with the energy of incident light, different depths of the sample can be probed by measuring LPV at different wavelengths and it can be found if the surfaces have any role to play in LPV. The LPV measurement at different wavelengths in the presence of strong bias light is also expected to reveal if surface band bending plays any significant role in LPV. LPV can

also be measured with chopped light and its frequency dependence may help us in understanding the recombination mechanism.

On the theoretical side, it would be desirable to construct a model to correlate LPV with the width of potential. This could be done by computer simulation in a manner similar to the one used in the analysis of conductivity and thermopower data [24].

LPV appears to be powerful tool to compare the heterogeneities present in different samples. However, a more detailed study needs to be done to be sure of the efficacy of this approch.

To summarize we can say that a lot of interesting physics remains to be studied in a-Si:H vis-á-vis Lateral Photovoltage and both experimental as well as theoretical work is required in order to understand LPV reasonably well.

APPENDIX

A

Transmission Measurement

Assuming that the substrate is non-absorbing and $K = 0$ which is true for most part of the spectrum we have [96]

$$T = \frac{Ax}{(B - Cx\cos\phi + Dx^2)}. \tag{A.1}$$

where

$$A = 16n^2 s, \tag{A.2}$$

$$B = (n+1)^3(n+s^2), \tag{A.3}$$

$$C = 2(n^2-1)(n^2-s^2), \tag{A.4}$$

$$D = (n-1)^3(n-s) \tag{A.5}$$

$$\phi = 4\pi nd/\lambda \tag{A.6}$$

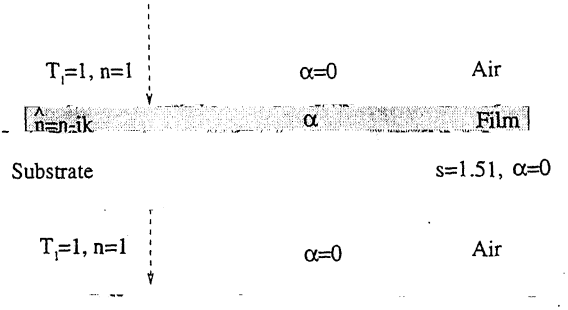

Figure A.1: The schematic shows the transmission geometry of a-Si:H thin film on a non-absorbing substrate

$$x = exp(-\alpha d). \tag{A.7}$$

The symbols are defined in the Fig. A.1. Fig. A.2 shows the transmission spectrum of an a-Si:H thin film. T_M and T_m are envelopes of maxima and minima of the interference fringes.

Determination of $n(\lambda)$

The refractive index $n(\lambda)$ of a-Si:H thin film is given by different expression in the different regions of the transmission spectrum. The transmission spectrum can be divided into three regions: (i) the transparent region ($T_M > 0.9$), (ii) weak and medium absorption region ($0.9 \geq T_M \geq 0.5$) and (iii) a strong absorption region ($T_M > 0.5$). The absorption coefficient α is given in the closed forms [96].

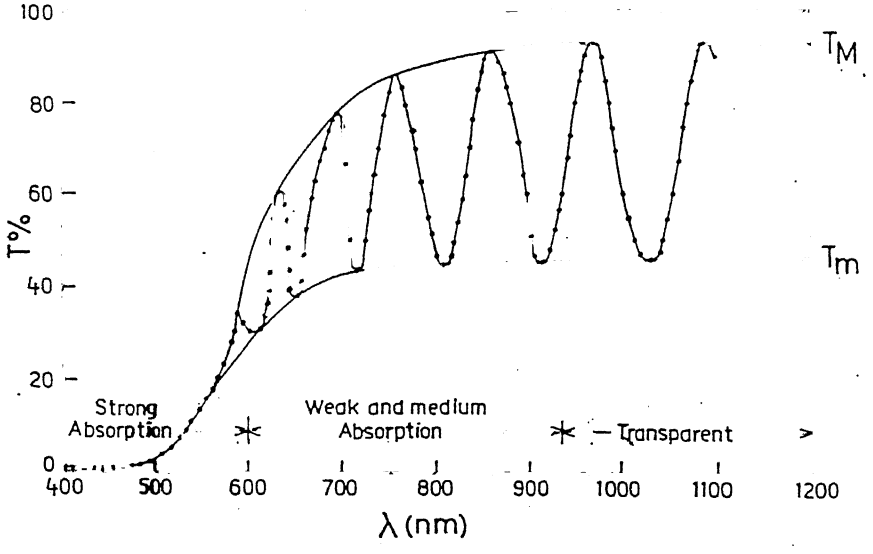

Figure A.2: Tranmission spectrum of a-Si:H thin film on 7958 glass substrate.

The transparent region

$$n = (M + (M^2 - s^2)^{1/2})^{1/2}. \tag{A.8}$$

where $M = (2s/T_m) - (s^2 + 1)/2$ and $\alpha = 0$.

Weak and medium absorption

$$n = (N + (N^2 - s^2)^{1/2})^{1/2}. \tag{A.9}$$

where

$$N = 2s\frac{(T_M - T_m)}{T_M T_m} - \frac{s^2 + 1}{2}$$

and

$$x = \frac{F - (F^2 - (n^2-1)^3(n^2-s^4))^1/2}{(n-1)^3(n-s^2)} \tag{A.10}$$

where

$$F = \frac{4n^2 s(T_M + T_m)}{T_M T_m}$$

The strong absorption region

As seen from the Fig. A.1, there is no interference fringes in the transmission spectrum in this region, $n(\lambda)$ is calculated by the extrapolation of $n(\lambda)$ obtained in the other two regions. using the Cauchy's relation

$$n(\lambda) = A + B/\lambda^2 \tag{A.11}$$

and

$$x = \frac{(n+1)^3(n+s^2)}{16n^2 s} T_0 \tag{A.12}$$

where $s = 1.51$ is the refractive index of the 7059 glass and T_0 is the measured transmission in the interference free region (Fig. A.2).

Determination of α

The values of the refractive index $n(\lambda)$ calculated for different regions are used to calculate the values of x in the respective region. Now using $x = exp(-\alpha d)$ the values of α can be obtained as a function of wavelength.

The optical gap of the film is obtained from straight line region of the plot of $\sqrt{(\alpha h\nu)}$ vs $h\nu$ as in this region

$$\sqrt{(\alpha h\nu)} = A \times (h\nu - E_g). \tag{A.13}$$

From this graph, E_g is the intercept of the straight line on the energy axis.

BIBLIOGRAPHY

[1] H. F. Sterling and R. C. G. Swann. Solid State Electr. **8**, 653 (1965).

[2] R. C. Chittick, J. H. Alexander and H. F. Sterling. J. Electrochem. Soc. **116**, 77 (1969).

[3] A. Triska, D. Dennison and H. Fritzsche. Bull. Am. Phys. Soc. **20**, 392 (1975).

[4] H. Fritzsche. In *Proc. 7th Int. Conf. on Amorphous and Liquid Semiconductors*, W. E. Spear, ed., p. 3 (CICL, Edinburg, 1977).

[5] W. E. Spear and P. G. LeComber. Phil. Mag. **33**, 935 (1976).

[6] W. E. Spear, P. G. LeComber, S. Kinmond and M. H. Brodsky. Appl. Phys. Lett. **28**, 105 (1976).

[7] P. G. LeComber, A. Madan and W. E. Spear. J. Non-Cryst Solids **11**, 219 (1972).

[8] D. E. Carlson and C. R. Wronski. Appl. Phys. Lett. **28**, 671 (1976).

[9] D. L. Staebler and C. R. Wronski. Appl. Phys. Lett. **31**, 292 (1977).

[10] Mehmet Güneş and Christopher R. Wronski. J. Appl. Phys. **80**, 3526 (1997).

[11] D. L. Steabler. In *Amorphous and Microcystalline Silicon Technology*, Michael Hack, Eric Schiff, Ruud Schropp, Isamu Shimizu and Sigurd Wagner, eds., **467**, p. 3 (MRS, Warrendale, PA, USA, 1997).

[12] C. R. Wronski. In *Amorphous and Microcystalline Silicon Technology*, Michael Hack, Eric Schiff, Ruud Schropp, Isamu Shimizu and Sigurd Wagner, eds., **467**, p. 7 (MRS, Warrendale, PA, USA, 1997).

[13] H. Fritzsche. In *Amorphous and Microcystalline Silicon Technology*, Michael Hack, Eric Schiff, Ruud Schropp, Isamu Shimizu and Sigurd Wagner, eds., **467**, p. 19 (MRS, Warrendale, PA, USA, 1997).

[14] H. Fritzsche. Ann. Rev. of Mat. Sci. (to appear).

[15] N. F. Mott and E. A. Davis. *Electronic Process in Non-Crystalline Materials*, Chapter 2 and 6. 2nd edition (Clarendon Press, Oxford, 1979).

[16] M.H. Cohen, H. Fritzsche and S.R. Ovshinsky. Phys. Rev. Lett. **22**, 1065 (1969).

[17] H. Overhof and P. Thomas. *Electronic Transport in Hydrogenated Amorphous Semiconductors*, Vol. **114** (Springer–Verlag, Berlin, 1989).

[18] H. Fritzsche. J. Non-Cryst. Solids **6**, 49 (1971).

[19] J. C. Knights and R. A. Reimer. Appl. Phys. Lett. **35**, 244 (1979).

[20] P. D'Antionio and J. H. Konnart. Phys. Rev. Lett. **43**, 1161 (1979).

[21] J. A. Reimer and M. A. Patrich. In *Amorphous Silicon and Related Materials*, H. Fritzsche, ed., Vol. **A**, p. 3 (World Scientific, Singapore, 1989).

[22] R. A. Reimer, R. W. Vaughan and J. C. Knights. Phys. Rev. Lett. **44**, 193 (1980).

[23] S. D. Baranovskii and M. Silver. Phil. Mag. Lett. **61**, 77 (1990).

[24] H. Overhof and W. Beyer. Phil. Mag. **B 43**, 433 (1981).

[25] M.H. Brodsky. Solid State Commun. **36**, 55 (1980).

[26] H. Fritzsche. J. Non-Cryst. Solids **59–60**, 398 (1983).

[27] J. A. Howard and R. A. Street. Phys. Rev. **B 44**, 7935 (1991).

[28] Yi Tang and R. Braunstein. Appl. Phys. Lett. **66**(1), 721 (1995).

[29] Yi Tang, S. Dong and R. Braunstein. Appl. Phys. Lett. **68**(5), 640 (1996).

[30] S. C. Agarwal. Indian. J. Pure and Applied Phys. **34**, 597 (1996).

[31] Pratima Agarwal and S. C. Agarwal. Solid State Phenomena **55**, 140 (1997).

[32] Pratima Agarwal and S. C. Agarwal. Phil. Mag. **B 80**, 1327 (2000).

[33] Pratima Agarwal and S. C. Agarwal. J. Appl. Phys. **81**, 3214 (1997).

[34] A. K. Sinha and S. C. Agarwal. J. Vac. Sci. Technol. **B 18**(3), 1805 (May/June 2000).

[35] R. A. Street, J. Zesch and M. J. Thompson. Appl. Phys. Lett. **43**, 772 (1983).

[36] J. D. Cohen, J. P. Habrison and K. W. Wecht. Phys. Rev. Lett. **48**, 109 (1982).

[37] W. E. Spear and P. G. LeComber. J. Non-Cryst. Solids **8-10**, 727 (1972).

[38] D. S. Misra, A. Kumar and S. C. Agarwal. Phil. Mag **B49**, L69 (1984).

[39] D. S. Misra, A. Kumar and S. C. Agarwal. Phys. Rev. **B31**, 1047 (1985).

[40] D. S. Misra, V. A. Singh and S. C. Agarwal. Sol. Stat. Comm. **55**, 147 (1985).

[41] D. S. Misra, V. A. Singh and S. C. Agarwal. Phys. Rev. **B32**, 4052 (1985).

[42] D. S. Misra, A. Kumar and S. C. Agarwal. J. Non-Cryst. Solids **76** 215 (1985).

[43] D. S. Mishra. Ph. D. Thesis, I.I.T., Kanpur (1984).

[44] S. Ashok and S. J. Fonash. IEEE, Electron Devices **ED-1**, 200 (1980).

[45] P. Viktorovich and D. Moddel. J. Appl. Phys. **E1**, 4847 (1980).

[46] M. Vanecek, J. Stuchlik J. Kocka, Z. Koicek, O. Stika and A. Triska. Solar Energy Materials **8**, 411 (1983).

[47] W. B. Jakson, N. M. Amer, A. C. Boccara and D. Fournier. Appl. Optics **20**, 1333 (1981).

[48] W. B. Jackson and N. M. Amer. Phys. Rev. **B 25**, 5559 (1982).

[49] S. C. Agarwal, J. S. Payson and S. Guha. Phys. Rev. **B36**, 9348 (1987).

[50] A. K. Sinha, M. Malhotra, S. Kumar, E. Bhattacharya and S. C. Agarwal. Ind. J. Pure and Appl. Phys. **31**, 548 (1993).

[51] W. H. Brattain. Phys. Rev. **72**, 354 (1947).

[52] W. H. Brattain and J. Bardeen. Bell System Tech. J. **32**, 1 (1953).

[53] J. Dresner, D. J. Szostak and B. Goldstein. Appl. Phys. lett. **38**, 998 (1981).

[54] A. R. Moore. Appl. Phys. lett. **40**, 403 (1982).

[55] A. R. Moore. J. Appl. Phys. **54**, 222 (1983).

[56] A. R. Moore and H.-S. Lin. J. Appl. Phys. **61**, 4816 (1987).

[57] S. Kumar and S. C. Agarwal. Phil. Mag. **B 49**, 453 (1984).

[58] Shailendra Kumar and S. C. Agarwal. Phil. Mag. **B 49**, L53 (1984).

[59] Shailendra Kumar. Ph. D. Thesis, I.I.T., Kanpur (1984).

[60] Shailendra Kumar and S. C. Agarwal. Appl. Phys. Lett **45**, 575 (1985).

[61] Shailendra Kumar and S. C. Agarwal. J. Appl. Phys. **58**, 3798 (1985).

[62] L. Kronik and Y. Shapira. Surface Science Reports **37**, 1 (1999).

[63] G. Lucovsky. J. Appl. Phys. **31**, 1088 (1960).

[64] D. J. W. Noorlag and S. Middelhoek. Solid State Electron Devices **3**, 75 (1979).

[65] W. P. Connors. IEEE Trans. Electron Devices **ED-18**, 591 (1971).

[66] H. J. Woltring. IEEE Trans. Electron Devices **ED-22**, 581 (1975).

[67] R. Martins, M. Vieira, F. Soares and L. Guimaraes. Proc. 5^{th} International Photovoltaic Conference p. 975 (1990).

[68] M. Vieira, R. Martins, F. Soares and L. Guimaraes. J. Non. Cryst. Solids **137-138**, 479 (1991).

[69] R. Martins and E. Fortunato. Rev. Sci. Instrum. **66**, 2927 (1995).

[70] E. Fortunato, I. Ferreira, F. Giuliani, P. Wurmsdobler and R. Martins. J. Non-Cryst. Solids **266-269**, 1213 (2000).

[71] M. Tucci, R. De Rosa, F. Roca, D. Caputo and G. de Cesare. J. Non-Cryst. Solids **266-269**, 1218 (2000).

[72] Alok Srivastava and S. C. Agarwal. In *Preceedings of the DAE Solid state physics symposium*, **39C**, p. 428 (BARC, Bombay, India, 1996).

[73] Alok Srivastava and S. C. Agarwal. In *Proceedings of the 4th National Seminar on the Physics and Technology of Sensors*, N. G. Patel, K. K. Makhija, R. N. Karekar and S. A. Gangal, eds., p. P8 (Sardar Patel University, Anand, India, 1997).

[74] Alok Srivastava and S. C. Agarwal. J. Non. Cryst. Solids **227-230**, 259 (1998).

[75] J. I. Pankov. *Optical Processes in Semoconductors* (Prantice Hall, Inc., New Jersey, 1971).

[76] D. Ritter, K. Weiser and E. Zeldov. J. Appl. Phys. **62**, 4563 (1987).

[77] K. Weiser and D. Ritter. In *Amorphous Silicon and Related Materials*, H. Fritzsche, ed., Vol. **B**, pp. 871–883 (World Scientific, Singapore, 1989).

[78] I Sakata, M. Yamanaka and T. Sekigawa. J. Appl. Phys **82**(3), 1323 (1997).

[79] B. Goldstein and L. Pensak. J. Appl. Phys. **30**, 155 (1959).

[80] M. Kamiyama, M. Haradome and H. Kukimoto. Japanese. J. Appl. Phys. **1**, 202 (1962).

[81] G. Ellis, E. E. Loebner, W. J. Merz, C. W. Struck and J. G. White. Phys. Rev. **109**, 180 (1958).

[82] W. J. Mertz. Helvetica Phisica Acta **31**, 625 (1958).

[83] W. Ruppel and P. M. Grant. Solid State Comm. **4**, 649 (1966).

[84] E. I. Adrirovich, T. Mirzamakhmudov, V. M. Rubinov and Yu. M. Yuabov. Sov. Phys. – Solid State **7**, 2946 (1966).

[85] H. Dember. Physik. Zeits **32**, 554 and 856 (1931).

[86] H. Dember. Physik. Zeits **33**, 209 (1932).

[87] W. Schottky. Z. Phys. **31**, 913 (1930).

[88] J. T. Wallmark. Proc. IRE **45**, 474 (1957).

[89] J. I. Alferov, V. M. Andreen, E. L. Portnoi and I. I. Portasov. Sov. Phys. – Semiconductors **3**, 1103 (1970).

[90] É. I. Adirovich, V. M. Rubinov and Yu. M. Youbov. Sov. Phys. Dokl. **10**, 844 (1966).

[91] D. S. Misra, P. N. Dixit and S. C. Agarwal. Bull. Mater. Sci. **3**, 347 (1981).

[92] A. Matsuda and N. Hata. In *Glow–Discharge Hydrogenated Amorphous Silicon*, K. Tanaka, ed., pp. 9–38 (KTK Scientific Publishers, Tokyo, 1989).

[93] C. C. Tsai. In *Amorphous Silicon and Related Materials*, H. Fritzsche, ed., Vol. **A**, pp. 123-147 (World Scientific, Singapore, 1989).

[94] W. Luft and Y. S. Tsuo. *Hydrogenated Amorphous Silicon Aloy Deposition Processes*, Chapter 7, pp. 145–161 (Marcel Dekker Inc., New York, USA, 1993).

[95] H. Fritzsche, M. Tanielian, C. C. Tsai and P. J. Gaczi. J. Appl. Phys. **50**, 3366 (1979).

[96] R. Swanpole. J.Phys. **E 16**, 1214 (1983).

[97] J. Kočka, M. Vaněček and A. Tříska. In *Amorphous Silicon and Related Materials*, H. Fritzsche, ed., Vol. **A**, pp. 297–327 (World Scientific, Singapore, 1989).

[98] R. S. Crandall. In *semiconductor and Semimetals*, J. I. Pankov, ed., Vol **21B**, p. 289 (Academic Press, Orlando, 1989).

[99] D. E. Carlson, A. R. Moore and A. Catalano. J. Non. Cryst. Solids **66**, 59 (1984).

[100] K. A. Epstein, N. T. Tran, F. R. Jeffrey and A. R. Moore. Appl. Phys. lett. **49**, 173 (1986).

[101] R. Schwarz, D. Slobodin and S. Wagner. Appl. Phys. lett. **47**, 740 (1985).

[102] S. R. Kurtz, J. Proscia and R. Gordon. J. Appl. Phys. **59**, 249 (1986).

[103] R. Schwarz, S. Goedecker, T. Muschik, N. Wyrschik and A. V. Shah. J. Non-Cryst. Solids **97-98**, 759 (1987).

[104] I. Sakata, T. Isida, S. Okasaki, T. Saitoh, M. Yamanaka and Y. Hayasaki. J. Appl. Phys. **61**, 1916 (1987).

[105] H. J. Eichler. Adv. in Solid State Physics **28**, 241 (1978).

[106] S. Kumoro, Y. Aoyagi, Y. Segawa, S. Namba, A. Masuyama, H. Okamoto and Y. Hamakawa. Appl. Phys. Lett. **42**, 79 (1983).

[107] K. Hatori, T. Mori, H. Okmoto and Y. Hamakawa. Appl. Phys. lett. **51**, 1259 (1987).

[108] V. J. Newell, T. S. Rose and M. D. Fayer. Phys. Rev. **32B**, 8035 (1986).

[109] D. Ritter, E. Zeldov and K. Weiser. Appl. Phys. lett. **49**, 791 (1986).

[110] R. A. Smith. *Semiconductors*, Chapter 7 (Cambrigde University Press, U. K., 1987).

[111] J. A. Reimer, R. W. Vaughan and J. C.Knights. Phys. Rev. **B23**, 2567 (1981).

[112] A. J. Hamed. Phys. Rev. **B44**, 5585 (1991).

[113] S. Dong, Y. Tang, R. Braunstein, R. S. Crandall, B. P. Nelson and A. H. Mahan. J. Appl. Phys. **82**(2), 4047 (July 1997).

[114] J. A. Schmidt, M. Cutrera, R. H. Buitrago and R. D. Arce. Appl. Phys. Lett. **26**, 4047 (1996).

[115] P. Tzanetakis, H. Fritzsche, M. Q. Tran, M. Androulidaki and E. Rynes. J. Non. Cryst. Solids **164-166**, 607 (1993).

[116] D. Hauschildt, W. Fuhs and H. Mell. Phys. Stat. Solidi **B 111**, 171 (1982).

[117] P. Agarwal, S. K. Tripathi, S. Kumar and S. C. Agarwal. J. Non-Cryst. Solids **201**, 163 (1996).

[118] J. Z. Liu, X. Li, P. Roca i Cabarrocas, J. P. Conde, A. Mayurama, H. Park, S. Wagner and A. E. Delahoy. IEEE PV Spec. Conf. Proc. p. 1606 (1990).

[119] Y. S. Tsuo, Y. Xu, E. A. Ramsay, S. J. Salamon, R. S. Crandall, I. Balberg B. P. Nelson, Y. Xiao and Y. Chen. Mat. Res. Soc. Symp. Proc. **219**, 769 (1991).

[120] W. Luft and Y. S. Tsuo. *Hydrogenated Amorphous Silicon Aloy Deposition Processes*, Chapter 2 (Marcel Dekker Inc., New York, USA, 1993).

List of Publications

1. *Potential fluctuations, diffusion length, and lateral photovoltage in hydrogenated amorphous silicon and silicon germanium thin films*, Alok Srivastava and S.C. Agarwal, *Phys. Rev.* (Communicated).

2. *Lateral Photovoltage in Hydrogenated Amorphous Silicon*, Alok Srivastava and S.C. Agarwal, *J. Non. Cryst. Solids*, **237-230**, 259 (1998).

3. *Ambipolar Diffusion length and Lateral Photovoltage Measurements in Hydrogenated Amorphous Silicon*, Alok Srivastava and S.C. Agarwal, *DAE SSP Symposium* **43C** (2000) (Accepted).

4. *Residual Stess in Diamond Films using Raman Spectroscopy*, G. S. Narayana, S. K. Tripathi, Alok Srivastava, A. K. Sinha and S.C. Agarwal, *Indian J. Phys.* **73S** 161 (1999).

5. *Position Sensitive Detector using Hydrogenated Amorphous Silicon*, Alok Srivastava and S.C. Agarwal, 4^{th} National Seminars on Physics and Technology of Sensors P8 (1997).

6. *Role of Hydrogen on the electrical transport properties of porous silicon*, Alok Srivastava and S.C. Agarwal in *Physics of Semiconductor Nanostructures* ed. K.P. Jain, Narosa Publishing House New Delhi, 155, 1997.

7. *Hydrogenated Amorphous Silicon Under Non–Uniform Illumination*, Alok Srivastava and S.C. Agarwal, *DAE SSP Symposium* **39C** 428 (1996).